UNIVERSITÀ POLITECNICA DELLE MARCHE

Master's Degree in Biomedical Engineering
Department of Information Engineering

Measuring and controlling thermal comfort in indoor environments through physiological parameters and machine learning

Supervisor:
Prof. Ing. Gian Marco Revel

Candidate:
Riccardo Naccarelli

Co-supervisors:
Dott. Ing. Sara Casaccia
Dott. Ing. Nicole Morresi

Academic Year 2019/2020

INDEX OF CONTENTS

LIST OF SYMBOLS

Symbol	Description
EDA	Electro-Dermal Activity [μS]
HF	High Frequency [Hz]
HR	Heart Rate [bpm]
HRV	Heart Rate Variability [s]
LF	Low Frequency [Hz]
PMV	Predicted Mean Vote [-]
PPD	Predicted Percentage of Dissatisfied [%]
PSD	Power Spectral Density [ms^2]
VLF	Very Low Frequency [Hz]

LIST OF ABBREVIATIONS

Abbreviation	Description
AI	Artificial Intelligence
ASHRAE	American Society of Heating, Refrigerating, and Air-Conditioning Engineers
ECG	Electrocardiogram
EEG	Electroencephalogram
HVAC	Heating, ventilation and air-conditioning
ISO	International Organization for Standardization
LR	Logistic Regression
ML	Machine Learning
NZEB	Near Zero Energy Building
PPG	Photoplethysmogram
RF	Random Forest
SVR	Support Vector Regression
TSV	Thermal sensation vote

LIST OF FIGURES

LIST OF TABLES

CHAPTER 1

INTRODUCTION

1.1 Aim of the study

The real-time perception of thermal comfort plays an important role in human-oriented smart buildings and their energy efficiency. A large part of buildings' energy consumption is related to HVAC systems. Feedback signals from thermal comfort perception of the occupants can be used to control and optimize HVAC energy consumption. Human thermal comfort is a subjective feeling that depends on how human body interacts with the environment, so the indoor environmental parameters can be controlled basing on thermal perception level of the occupant in order to reach the thermal comfort and to optimize the energy efficiency of the building. To this purpose, in recent years control algorithms able to predict the thermal comfort of the individuals inside a building are being developed. These algorithms use a machine learning (ML) based approach to learn the individual's thermal comfort model through different environmental factors and physiological features as input.

Considering the aforementioned purpose of reducing the energy consumption of HVAC systems in buildings and, at the same time, ensuring the thermal comfort of the occupants, the aim of this thesis is to develop a real-time acquisition system of environmental and human signals able to predict through a ML algorithm the occupant thermal sensation vote (TSV), and which is able to compute the optimal temperature setpoint for the HVAC system for restoring the comfort condition of the user. Currently, a method available to evaluate the thermal well-being of the person within an environment is through the TSV, an index that directly reflects the perceived level of comfort. This work is developed under the framework of the RenoZEB project, an EU-funded project under Horizon 2020 launched on 1 October 2017, whose goal is to unlock the NZEB Renovation market by increasing the value of the property through a new approach to modernization, including innovative decision-making components, processes and methodologies. In this context, the work presented aims to find a method that can better adapt the real-time measurement of thermal comfort to the physical needs of the person.

1.2 Thermal Comfort

Thermal comfort is defined as "The condition of mind that expresses satisfaction with the thermal environment and is assessed by subjective evaluation" [1]. From a physiological point of view, thermal comfort occurs when there is thermal equilibrium between a person's body and the environment. Different approaches are used to achieve thermal comfort with different limitations. The most common methods are the Fanger's method and the Adaptive one. The standards defined the thermal comfort using these two models, setting temperature ranges that resulted in thermal satisfaction for at least 80% of occupants in an indoor environment [1]. The international comfort standards such as ASHRAE and EN 15251 are mostly based on the analysis of human heat exchange done in different regions around the world. They were based on mathematical models developed by Fanger in studies from controlled climate chamber experiments. Among the limitations of these standards we find that they are only suitable for static and uniform thermal conditions and that they do not consider race, age and sex.

Thermal sensations can be expressed by a seven-point scale, the so called ASHRAE's thermal sensation scale (Figure 1). This scale provides a score that ranges from -3 to +3 which quantifies people's thermal sensation. The score that converges to zero reflects the maximum level of the occupant satisfaction in the environment while the score that converges to the scale limits reflects the lowest degree of comfort. The negative values are used to indicate cold sensations, the positive values to indicate hot ones and the zero to indicate the neutral sensation.

Thermal sensation	vote
+3	Hot
+2	Warm
+1	Slightly warm
0	Neutral
-1	Slightly cool
-2	Cool
-3	Cold

Figure 1. Seven-point ASHRAE's thermal sensation scale.

There are various factors which influence thermal comfort determining heat gain and loss, which can be grouped in three categories:

- **personal factors**, which reflect the characteristics of the occupant and include the metabolic rate and the clothing insulation;
- **environmental factors**, conditions of the thermal environment which include air temperature, mean radiant temperature, air speed and relative humidity;
- **physiological factors**, parameters related to the human body response (as the skin and internal temperatures), the sweat rate and the heart rate.

Metabolic rate is the level of transformation of chemical energy into heat and mechanical work by metabolic activities within the body which is expressed in met units (1 met = 60 W/m²). ASHRAE Standard provides a table of met rates for a variety of activities shown in Figure 2.

activity	met
sleeping	0.7
reclining, lying in bed	0.8
seated, at rest	1.0
standing, sedentary work	1.2
very light work (shopping, cooking, light industry)	1.6
medium light work (house~, machine tool ~)	2.0
steady medium work (jackhammer, social dancing)	3.0
heavy work (sawing, planing by hand, tennis) up to	6.0
very heavy work (squash, furnace work) up to	7.0

Figure 2. Metabolic rates associated to different activities.

Clothing insulation is the amount of thermal insulation worn by a person which is expressed in clo units (1 clo= 0.155 $m^2 \cdot K/W$). Generally, the thicker the garment, the greater insulating ability. Depending on the type of material the clothing is made of, air movement and relative humidity can decrease the insulating ability of the material.
In Figure 3 are reported the thermal insulations expressed in clo units related to different clothes.

Man		clo	Women		clo
underwear	singlets	0.06	underwear	bra + panties	0.05
	T-shirt	0.09		half slip	0.13
	briefs	0.05		full slip	0.19
	long, upper	0.35		long, upper	0.35
	long, lower	0.35		long, lower	0.35
shirt	light, short sleeve	0.14	blouse	light	0.20
	light, long sleeve	0.22		heavy	0.29
	heavy, short sleeve	0.25	dress	light	0.22
	heavy, long sleeve	0.29		heavy	0.70
	+5% for tie or turtle-neck)				
vest:	light	0.15	skirt	light	0.10
	heavy	0.29		heavy	0.22
trousers	light	0.26	slacks	light	0.26
	heavy	0.32		heavy	0.44
pullover	light	0.20	pullover	light	0.17
	heavy	0.37		heavy	0.37
jacket	light	0.22	jacket	light	0.17
	heavy	0.49		heavy	0.37
socks	ankle length	0.04	stockings	any length	0.01
	knee length	0.10		panty-hose	0.01
footwear	sandals	0.02	footwear	sandals	0.02
	shoes	0.04		shoes	0.04
	boots	0.08		boots	0.08

Figure 3. Thermal insulations expressed in clo units related to different clothes.

Air temperature is the average temperature of the air surrounding the occupant, with respect to location and time. According to ASHRAE standard, the spatial average considers the ankle, waist and head levels, which vary for seated or standing occupants.
Mean radiant temperature is the average temperature of a surface that exchange thermal radiation, and it depends on the material's ability to absorb or emit heat.
Air speed corresponds to the average velocity of the air surrounding the occupant, without regard to direction.

Relative humidity (RH) is the ratio of partial pressure and saturation pressure of the water vapor, at the same temperature and total pressure. While the human body has sensors within the skin that are efficient at feeling heat and cold, RH is detected indirectly. Sweating is an effective heat loss mechanism that relies on evaporation from the skin. However, at high RH the air has close to the maximum water vapor that it can hold, so evaporation, and therefore heat loss, is decreased. On the other hand, very dry environments (RH < 20-30%) are also uncomfortable because of their effect on the mucous membranes. The recommended level of indoor humidity is in the range of 30-60% in air-conditioned buildings.

1.3 Thermal comfort models

In this paragraph, the Fanger's PMV model and Adaptive model of thermal comfort are discussed. The Fanger's model combines the theories of heat balance with the physiology of thermoregulation to determine a range of comfort temperatures suitable for occupants while the Adaptive model has the goal of analysing the acceptability of the environment based on the occupant's behaviour and expectation. The former model proved to be accurate for air-conditioned buildings, the latter better predicts for naturally ventilated buildings.

1.3.1 Fanger's model

The heat balance approach is based on Fanger experiments [2] performed inside a controlled climatic chamber on students using a steady state heat transfer model. Fanger stated that the human body strives towards thermal equilibrium and proposed the following formula:

$$\begin{aligned} PMV = [0.303e^{-0.036M} + 0.028]\{M - W - 3.05 \cdot 10^{-3}[5733 - 6.99(M - W) - P_a] \\ - 0.42[(M - W) - 58.15] - 1.72 \cdot 10^{-5} M(5867 - P_a) \\ - 0.0014M(34 - t_a) - 3.96 \cdot 10^{-8} f_{cl}[(t_{cl} + 273)^4] \\ - f_{cl} h_c (t_{cl} - t_a)\} \end{aligned} \quad (1)$$

where M is the metabolic rate of the human body, determined by the magnitude of human physical activity, W is the human mechanic work, P_a is the partial pressure around human

body, t_a is the air temperature around human body, f_{cl} is the dressing area coefficient, t_{cl} is the temperature of outside surface of cloth, t_r is the mean radiant temperature of room, and h_c is the convective heat transfer coefficient. Fanger's model allows to calculate an index which describes the average vote of the building occupants, called Predicted Mean Vote (PMV). The PMV index is computed using the Fanger comfort equation for human body heat exchange, thus it is a function of air temperature, mean radiant temperature, air velocity, relative humidity, metabolic rate and clothing insulation. Fanger developed also an index for predicting the percentage of occupants that will be dissatisfied with the thermal comfort, the so-called Predicted Percentage of Dissatisfied (PPD), and related it to the PMV through the equation:

$$PPD = 100 - 95e^{[-(0.03353PMV^4 + 0.2179PMV^2)]} \quad (2)$$

In the relationship between PPD and PMV it is visible that the 5% of the occupants would be dissatisfied even among the most comfortable conditions (PMV = 0). PPD values changing according to PMV are shown in Figure 4.

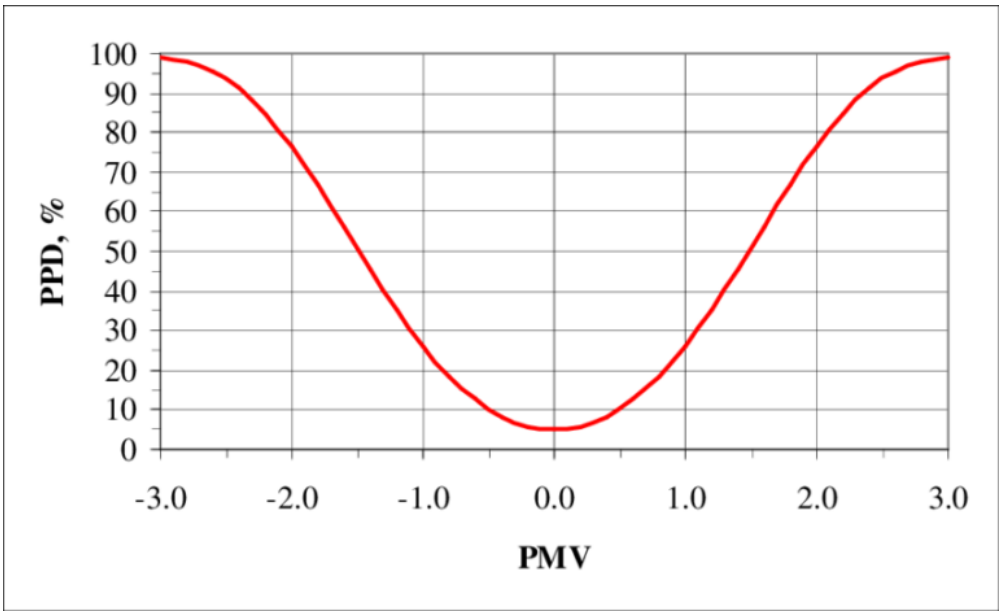

Figure 4. PPD relation with PMV.

Thermal comfort is considered at most between −0.5 and +0.5 given by the ISO 7730 and EN 15251 standards, but the closer the PMV value is to zero, the better the sensation of thermal comfort of the occupants.

The PMV model is the most used and is considered one of the best thermal comfort models for HVAC buildings, even if it does not take into account the sensations of the occupants or the external conditions by setting them as constant parameters.

1.3.2 Adaptive model

The adaptive model is based on studies conducted by de Dear and Brager [3] which show how the outdoor climate can affect indoor comfort as humans can adapt to different temperatures during different seasons of the year. The adaptive hypothesis predicts that by having access to past environmental controls and thermal history, it is possible to suppose the future thermal preferences of the building's occupants. It emerges from these studies that the occupants in naturally ventilated buildings accept a wider range of temperatures than the ones in air-conditioned buildings because their preferred temperature depends on outdoor conditions. These results were incorporated in the ASHRAE 55 standard as the Adaptive comfort model. The adaptive chart (Figure 5) relates indoor operative temperature to prevailing outdoor temperature and defines zones of 80% and 90% of satisfaction.

The human response to thermal distress has been summarized into three categories:

- behavioural adaptation: in naturally ventilated buildings, the occupants take numerous actions to keep themselves comfortable when the indoor conditions tends to discomfort (for example opening windows and changing clothing);
- physiological adaptation: the body has several thermal adjustment mechanisms to survive in different temperature environments (in a cold environment the body uses vasoconstriction, which reduces blood flow to the skin, skin temperature and heat dissipation, while in a warm environment, it uses vasodilation, which increases blood flow to the skin, skin temperature and heat dissipation);
- psychological adaptation: an individual's comfort level in each environment may change and adapt over time due to psychological factors (subjective perception of thermal comfort can be influenced by the memory of previous experiences).

The assumption behind the study is that people can control their environment in such a way as to try to achieve thermal comfort.

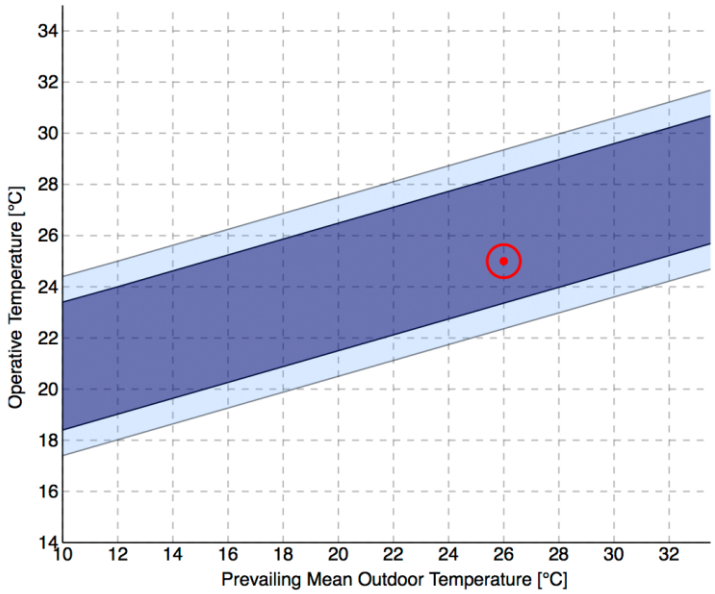

Figure 5. Adaptive chart according to ASHRAE Standard 55. It shows the relation between the operative temperature to the prevailing mean outdoor temperature and defines zones of 80% (light blue) and 90% (dark blue) of satisfaction.

1.4 Thermal Comfort Standards

In this paragraph the main international guidelines and standards on thermal comfort are discussed. The International Standard ISO 7730 [4] is based on Fanger's PMV, which predicts the mean thermal sensation of a group of people, and the PPD. The ASHRAE 55 standard [1] defines the conditions that are considered satisfactory for a specific percentage of users, including calculation methodologies for thermal comfort based on PMV and PPD. The EN 15251 [5] standard introduces classes of acceptability and suggests classifying thermal environments in small categories, distinguishing more satisfactory limit conditions.

1.4.1 ISO 7730

The purpose of this standard is to present a method for predicting the thermal sensation and the degree of thermal discomfort of people exposed to moderate thermal environments and to specify acceptable thermal environmental conditions for comfort. It can be used in the design of new environments or in evaluating existing ones. Thermal sensation is mostly related to the thermal balance of the person's body, but it is also

influenced by physical activity and clothing, as well as the environmental parameters (air temperature, mean radiant temperature, air velocity and air humidity). After these factors have been estimated or measured, the thermal sensation of the person can be predicted by calculating the PMV. The PPD instead provides information on thermal discomfort by predicting the percentage of people who are likely to feel too hot or too cold in an environment. An unwanted local cooling or heating of the body may also cause thermal discomfort. In this case the most common discomfort is draught, i.e. the local cooling of the body caused by air movement.

1.4.2 ASHRAE 55

The American Society of Heating, Refrigerating, and Air-Conditioning Engineers (ASHRAE) proposed a standard to specify the combinations of indoor environments and personal factors that leads to acceptable thermal environment conditions for most of the occupants.

The indoor environmental conditions are controlled by opening and closing windows, setting the air velocity using fans, or changing clothes. The standard establishes the ranges of these conditions defining areas within which more than 80% of occupants are satisfied with the thermal environment. These areas are defined through the equation:

$$T_{\text{accept}} = 0.31T_{\text{o}} + 17.8\ (°C\ or\ K) + T_{\text{lim}} \quad (3)$$

where T_{accept} (°C) represents the limits of the acceptable areas, T_o (°C) is the value of the mean outdoor temperature, T_{lim} = ± 3.5 K for 80% of satisfaction area and T_{lim} = ± 2.5K for 90% of satisfaction area. Acceptable limits of 80% are used for typical applications while 90% limits are used when a higher standard of thermal comfort is required. The indoor operative temperature (T_{op}) is expressed in (4) by the effect of air temperature (T_{air}) and mean radiant temperature (T_{mrd}), weighted by heat transfer coefficients by convection (h_{c}) and radiation (h_{r}).

$$T_{\text{op}} = (h_{\text{c}}T_{\text{air}}+h_{\text{r}}T_{\text{mrd}}) / (h_{\text{c}}+h_{\text{r}}) \quad (4)$$

1.4.3 EN 15251

The European Standard EN 15251 specifies the indoor environmental parameters which have an impact on the energy performance of buildings, including air quality, light and noise. It defines minimum ventilation requirements, minimum and maximum indoor temperatures that can be used for energy calculation, assessment and certification, but it does not include criteria for local discomfort factors like draught and vertical air temperature differences. EN 15251 is applicable mainly in non-industrial buildings, where the criteria for indoor environment are set by human occupancy, giving input parameters to the design of buildings, heating, cooling, ventilation and lighting systems.

1.5 Thermal comfort and body thermoregulation

The thermal well-being of the individual can be defined as the mental condition of satisfaction with the thermal environment and coincides with the state in which the subject does not feel hot or cold. The feeling of well-being is different from subject to subject and depends on factors such as metabolism, temperature, sex, clothing, age, activity, etc. Some are measurable environmental parameters and other non-quantifiable personal factors. Despite the large number of parameters that can influence it, at the basis of the thermal sensation of the human body is the temperature of the internal organs which, in healthy individuals, is around 37 °C, with a variation of about half a degree Celsius. Given the need to keep the internal temperature constant, the hypothalamus activates the thermoregulation system which is essentially of two types: vasomotor and behavioural. Depending on the external temperature, the hypothalamus dilates or constricts the blood vessels to increase or reduce the blood supply to the periphery. If this were not enough, the hypothalamus will switch to behavioural thermoregulation: sweating and reduced physical activity or chills and crouched body positions.

Most of the studies on thermal comfort aimed to bring the highest number of people into a state of well-being in a closed environment and were carried out in the workplace. It was found that a satisfactory thermal environment can improve working productivity. In a typical business building, the temperature is maintained according to the ASHRAE 55 standard between 20 °C and 24 °C in winter and between 24 °C and 27 °C in summer, but assumed that thermal comfort is a subjective feeling, some of the workers may not be in a well-being situation.

Much of the annual energy is used to maintain thermal comfort in the workplace, but despite this, a high percentage of workers are not satisfied. The researchers thus suggested to use a customized thermal comfort system for each worker which, unlike centralized systems, is capable of monitoring thermal comfort individually.
In hot or cold environments (discomfort), the perception of temperature and the response to it are synchronized by different neuronal pathways. Since thermoregulation is controlled by the nervous system, thermal comfort can be monitored by measuring the change in brain activity using, for example, an electroencephalogram. However, this strategy is hardly applicable in the real world. Also, the sensation could be implicitly monitored by recording other biological signals controlled by the nervous system. Furthermore, as body heat is transferred through the bloodstream, heart rate variability (HRV) has been proposed as a good indicator of thermal comfort [6]. Using the electrocardiogram, a recording of the electrical signal of the heart, it is possible to monitor the temporal fluctuations of heartbeats, i.e. the HRV.

1.6 Electrocardiogram

The electrocardiogram (ECG) is a diagnostic test that involves the use of an instrument capable of recording and graphically reproducing the rhythm and electrical activity of the heart. The heart is an organ composed of a muscle tissue called myocardium, whose peculiarity lies in the fact that it can generate and conduct nerve impulses for the contraction of the heart itself. These impulses (electrical signals) are generated at the level of the right atrium in a specific area called the sinoatrial node, capable of imposing the beat with a certain speed of contraction (heart rate). However, this frequency is variable as it is linked to the demand for blood by muscles and organs and to other stimuli that come from the human body. The nerves and muscles that make up the heart can be considered as a source of electrical charges that travel inside a conductor, the chest. The electric field produced by these moving charges emerges on the surface of the chest with its equipotential lines. Therefore, by placing on the thoracic surface special electrodes on two field lines with different potential, a potential difference can be detected. This potential difference varies over time with the depolarization and repolarization of the cardiac fibers, and its recording as a function of time takes the name of electrocardiogram.

1.6.1 Electrocardiographic waves

The ECG is composed by a succession of electric waves, each with typical characteristics that unite and distinguish them from other types of waves. The first deflection we find in an ECG track (Figure 6) is the P wave, corresponding to the depolarization of the atria. The subsequent waves, grouped in the so-called QRS complex, result from the depolarization of the ventricles: in particular the Q and S waves are negative deflections, while the R wave is a positive deflection. Finally, the T wave represents the repolarization of the ventricles. The repolarization of the atria, on the other hand, occurs during the PR interval or the QRS complex so it is not clearly identifiable.

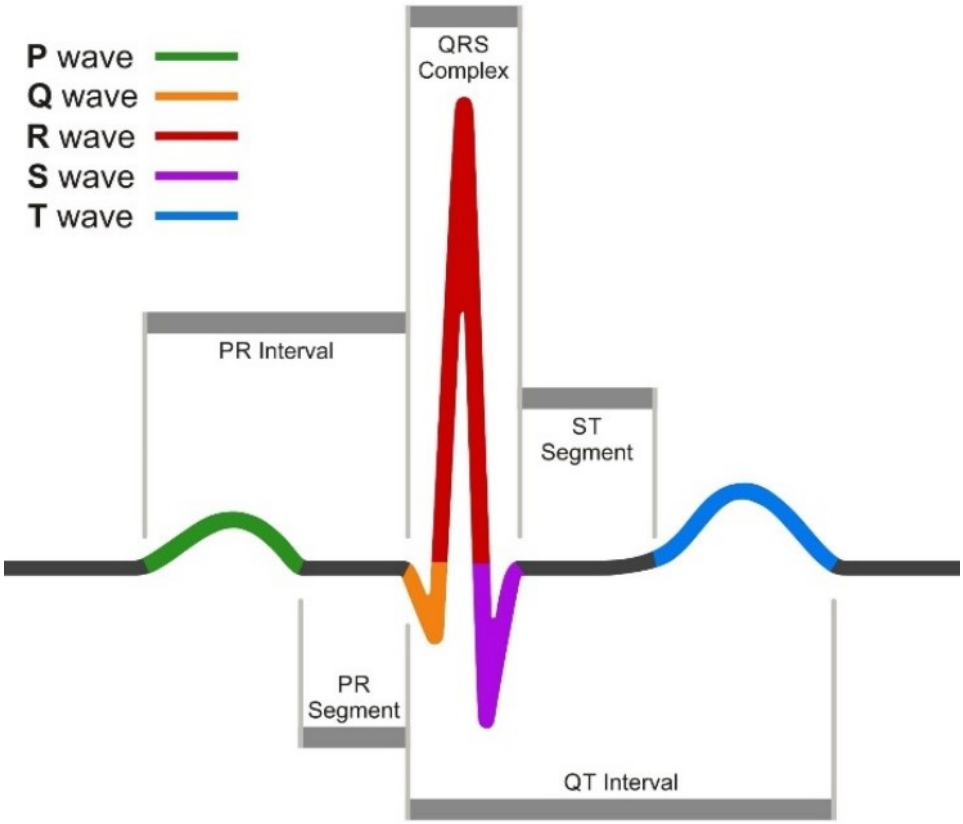

Figure 6. Trend of a cardiac cycle. Each wave is represented by a different colour reported in the legend, while each segment is properly highlighted.

1.7 Heart Rate Variability

HRV reflects the variation in time between two successive heartbeats. Heartbeat intervals, also called RR intervals, are not periodic, in fact the duration between two consecutive RR intervals varies from one heartbeat to another, as visible in Figure 7. This variation is not accidental and is linked to the human body's ability to maintain optimal conditions despite changes in external stimuli. The internal temperature of the human body is regulated by the hypothalamus which controls several mechanisms to increase or decrease the production of energy to restore the internal temperature through the action of the parasympathetic nervous system (PNS) and the sympathetic nervous system (SNS). These two have an opposite effect on heart rate: SNS increases heart rate, PNS decreases it [7].

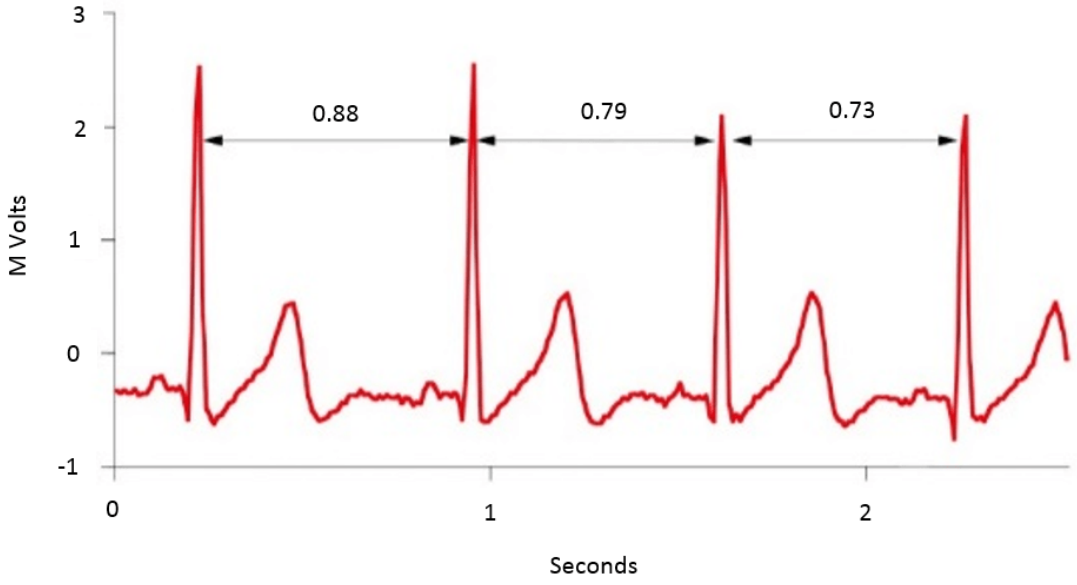

Figure 7. RR interval among successive heartbeats.

HRV is extracted from the ECG signal by identifying the QRS complex. It provides a precise measure of the variability of the RR interval and in particular indicates the degree of psycho-physical adaptability of the subject in response to various factors, such as breathing, physical stress, mental stress, pathologies, etc.

HRV can be analysed using different techniques, among which the time domain and frequency domain analysis. Before the analysis of the RR intervals there must be the removal of abnormal and ectopic beats (RR intervals that differ more than 20 – 25 % from the previous ones).

1.7.1 Time domain analysis

The time domain methods are the simplest to compute as they involve the detection, in an ECG recording, of the QRS complexes and therefore of the intervals between two beats. The series of these RR intervals constitutes the Tacogram (Figure 8), from which several measurements can be extracted. Figure 9 shows and describes all the time domain features that can be computed, classified in statistical measures and geometric ones.

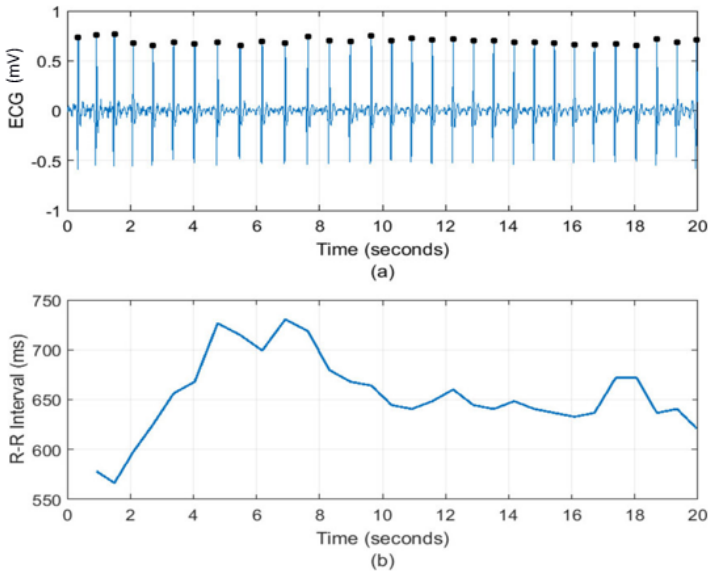

Figure 8. Tacogram (b), represented by RR interval series over time, extracted from the ECG (a).

Variable	Units	Description
Statistical measures		
SDNN	ms	Standard deviation of all NN intervals
SDANN	ms	Standard deviation of the averages of NN intervals in all 5-minute segments of the entire recording
RMSSD	ms	The square root of the mean of the sum of the squares of differences between adjacent NN intervals
SDNN index	ms	Mean of the standard deviations of all NN intervals for all 5-minute segments of the entire recording
SDSD	ms	Standard deviation of differences between adjacent NN intervals
NN50 count		Number of pairs of adjacent NN intervals differing by more than 50 ms in the entire recording; three variants are possible counting all such NN intervals pairs or only pairs in which the first or the second interval is longer
pNN50	%	NN50 count divided by the total number of all NN intervals
Geometric measures		
HRV triangular index		Total number of all NN intervals divided by the height of the histogram of all NN intervals measured on a discrete scale with bins of 7.8125 ms (1/128 seconds)
TINN	ms	Baseline width of the minimum square difference triangular interpolation of the highest peak of the histogram of all NN intervals
Differential index	ms	Difference between the widths of the histogram of differences between adjacent NN intervals measured

Figure 9. List of HRV parameters extracted through time domain analysis classified in statistical measures and geometric ones.

1.7.2 Frequency domain analysis

The approach in the frequency domain is based on the identification and quantification, in terms of frequency and power, of the main oscillatory rhythms of physiological origin that make up a sequence of RR intervals. It is possible to identify in a registration three main spectral frequency bands as reported in Figure 10:

- Very Low Frequency (VLF): 0.0033Hz to 0.04Hz;
- Low frequency (LF): 0.04Hz to 0.15Hz;
- High frequency (HF): from 0.15Hz to 0.4Hz.

The power spectrum of the HF band is influenced by the activity of the vagal nerve, while the power spectrum of the LF band refers mainly to the activity of the sympathetic nerve, instead the origin of the VLF band is unclear. Therefore, in the HRV analysis, the absolute power ratio in the LF and HF bands (LF/HF ratio) is considered an indicator of sympathetic/parasympathetic balance.

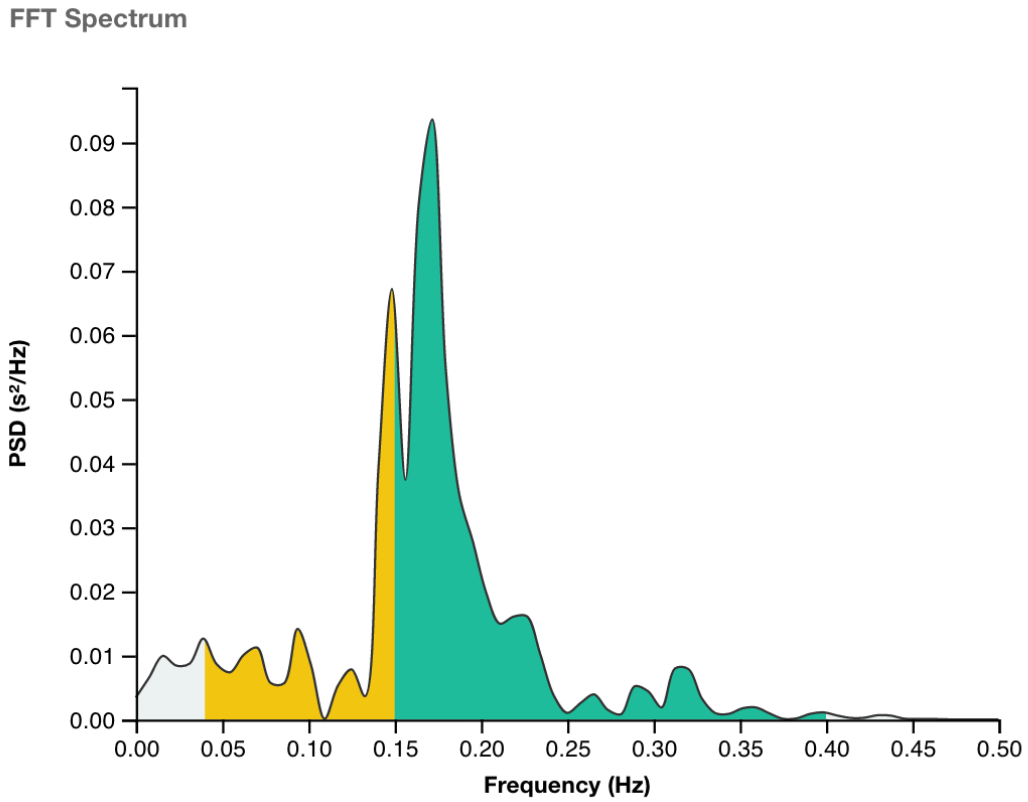

Figure 10. Spectral profile of a RR time series showing the PSD and its decomposition into VLF (grey area), LF (yellow area) and HF (green area) spectral components.

A method capable of detecting and measuring the peculiar aspects of cardiac rhythm dynamics is the Poincaré plot (Figure 11), which provides a visual and quantitative characterization of cardiac variability. It consists in representing each RR interval on a graph as a function of the previous one, obtaining a cloud of points arranged around the identity line. The cloud is characterized by two parameters: SD1 and SD2, which are indicative of short- and long-term cardiac variability respectively. The dispersion of the points in a perpendicular direction with respect to the identity line reflects short-term variability. In general, a greater dispersion of the points is associated with a correct balance of the autonomic nervous system, while a lesser dispersion is associated with an imbalance with a predominance of sympathetic activity [8].

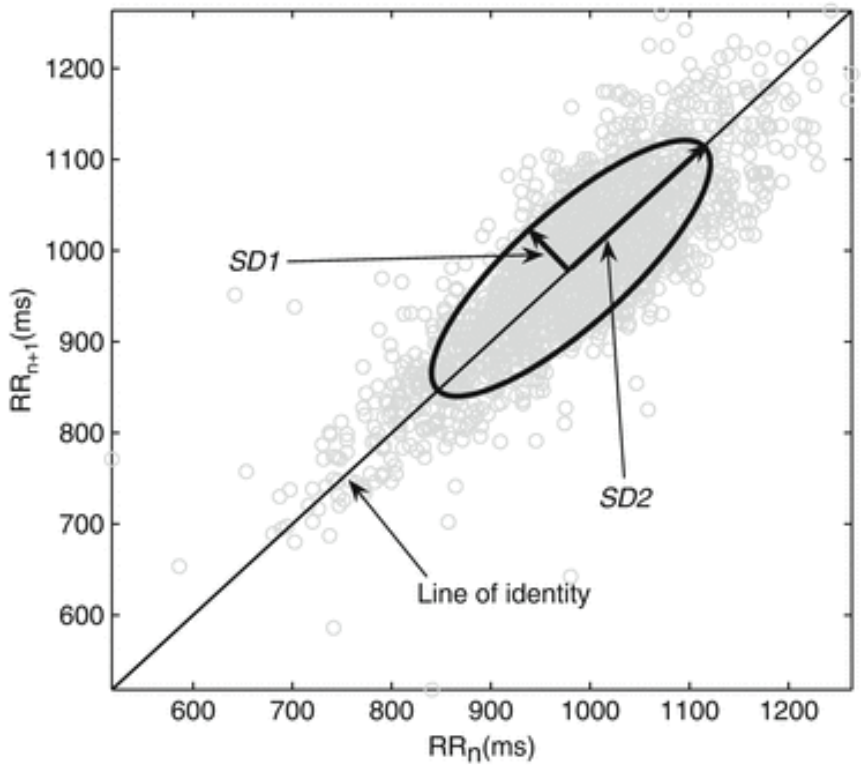

Figure 11. Poincaré plot.

CHAPTER 2

STATE OF THE ART

The aim of this project is to develop a real-time acquisition system of environmental and human signals able to predict through a ML algorithm the occupant thermal comfort, and which is able to compute the optimal ambient temperature. To do this, it was first necessary to highlight all the possible alternatives regarding the parameters to include in the prediction algorithm, the sensors to collect them and the learning model itself, thus a literature research was carried out. It was found that six main factors influence thermal comfort by determining heat gain and loss, which can be grouped into two categories: personal factors (characteristics of the occupant), which include metabolic rate and clothing insulation, and environmental factors (conditions of the thermal environment), which include air temperature, mean radiant temperature, air speed and relative humidity. Several studies have highlighted how the thermal sensation of users further depends on factors linked to human characteristics, for example age, gender and pathologies. There are currently two main approaches to assess thermal comfort: the rational method and the adaptive method. The first represents the standard method used to predict thermal comfort in steady state conditions and it is based on the use of Fanger's equations [9]. It combines above mentioned environmental and individual variables to give as result the PMV, an index that indicates how the occupants judge the climate. Using PMV, the PPD, that expresses the percentage of dissatisfied as a function of thermal sensation perceived by the users in the environment, can be then calculated. The other approach that can be used to predict thermal comfort is the Adaptive one, based on the subjective response of individuals to thermal stimuli and in which the main object of the analysis is the final users' satisfaction, that allows to optimize the thermal acceptability of the indoor environment. However, it has been proved that these two approaches have a low predicting power [10,11] because the effects of individual difference in physiological, psychological and behavioural factors are not considered.

Tracking human perception thermal comfort variations mainly involves three types of data collection methods. One is based on the use of questionnaires, in which the thermal preference of an occupant is collected and used as a basis for the regulation of environmental parameters, with the drawback of a continuous and frequent updating of

them. Another one is the environmental measurement method, which uses different sensors to measure indoor parameters like temperature, humidity and air flow. The last method is based on the collection through different sensors of the physiological parameters of the occupant. Among the latter the parameters which resulted from literature to be related to thermal comfort are skin temperature, skin conductance, heart rate, brain electrical waves, blood oxygen saturation and blood pressure. Many researchers examined thermal comfort in a multi-domain approach, including many of these, developing personal comfort models which predict individual's thermal comfort responses, instead of the average response of a large population. Furthermore, the personal comfort models considering personal factors achieved a higher predicting power than PMV and adaptive ones.

Human skin is the intermediary heat transmitter, so skin temperature and conductance play a fundamental role in thermoregulation controlled by dermal heat receptors through sweat emission, vasoconstriction and vasodilation. Sweat secretion and the related changes in skin conductance are nonconscious phenomena that are under the sympathetic control and reflect changes in arousal. Many studies showed important relations between skin temperature and thermal sensation, and proposed methods to predict thermal comfort based on skin temperature. In the study of Yu et al. [12] it is visible how local surface temperature detection of human body reflects the thermal comfort degree of the subject, and how from a measurement and calculation method point of view it is relatively simple and convenient to obtain it. Liu et al. [13] predicted personal thermal preference with an average accuracy of 75%, based on physiological signals (including skin temperatures at wrist and ankle) and environmental data. Dai et al. [14] predicted the thermal comfort requests of the individual occupants through SVM analysis. The skin temperature values of different points of the body were the only inputs for the model. It emerged that using a single skin temperature the prediction accuracy was the 80% of thermal demand, while using combined skin temperatures from different body segments the prediction accuracy improved to over 90%. Thermal adaptive changes were also observed by Maiti [15] through the distribution of local skin temperature and sweating at different temperatures. Skin conductance on the other hand, also called Electro-Dermal Activity (EDA), is useful to quantify sympathetic nervous system variations linked to changes in emotions and thermal sensations. The studies of Gerrett et al. [16,17] demonstrated a strong relationship between wetness sensation, EDA and thermal comfort. The latter proved to be influenced

by sweat during exercise in moderate-to-hot conditions, while EDA strictly monitored the process of sweat production, proving to be a good predictor of thermal comfort in all conditions and particularly during high sweat production. Also, different EDA responses between genders were observed, with females generally being more sensitive to sweat and warm thermal stimuli than males. Other studies used EDA to evaluate the arousal level of the patients [18], to quantify stress [19,20] and to classify emotional states [21], while there is not enough research about EDA related to thermal sensation.

Blood oxygen saturation (SpO_2), i.e. the percentage of haemoglobin binding sites in the bloodstream occupied by oxygen, is linked to respiration and can indicate the influence of thermal stimuli on the respiratory system. Another parameter linked to thermoregulation and that can reproduce the effect of thermal stress on the cardiovascular system is blood pressure. Xiong et al. studied the responses of SpO_2, blood pressure, skin temperature and heart rate to changes in temperature, finding in [22] that respiration, sweating and heart rate were accelerated in that situation, while in [23] and [24] that blood pressure, heart rate and skin temperature were sensitive to unexpected temperature changes.

The ECG is another important physiological indicator of thermal comfort status. Heart rate is in fact under the control of the autonomic nervous system, that is responsible for its changes necessary to restore the thermal equilibrium. HRV, the variation in the time interval between consecutive heartbeats, is the most important factor that can be extracted from the ECG. Heartbeat interval is called RR interval, since R peaks in the ECG waveform are used as a sign of the incidence of a heartbeat. The extraction of RR intervals from ECG can require considerable processing, especially because some measurements are counterfeit (ectopic beats) or noisy. After normal beats are extracted, the intervals measured are called NN intervals and so the HRV can be derived from them. Generally, HRV is analysed through two approaches: the time domain and the frequency domain analysis. In time domain there are geometric methods and statistical methods, which involve calculations such as the standard deviation of NN intervals (SDNN) or the square root of the mean squared differences of successive NN intervals (RMSSD). Frequency domain methods differentiate between extracting short-term spectral components (5 minutes interval) and long-term spectral analysis (24 hours interval). The ratio between low frequency (LF) and high frequency (HF) components (LF/HF) are among the short-term components, while a long-term indicator is the slope of the spectrum of a 24 hours

interval. HRV is related to the regulation of cardiac functions and it is responsive to modulations in sympathetic and parasympathetic nervous system, so many researchers included it in their thermal comfort prediction models as a variable sensitive to thermoregulation. The study of Nkurikiyeyezu et al. [25] suggests that it is possible to design automatic real-time thermal comfort controllers based on people's HRV, since they reached up to 93.7% accuracy in thermal comfort prediction. In another study [26] they used a photoplethysmographic signal recorded by a wristband, from which they extract the HRV time domain features to predict the user's thermal state in real-time, reaching through a Random Forest algorithm an accuracy exceeding 90%. They also observed that among time domain features few of them (mean RR, median RR and HR) were more important for thermal comfort prediction. As reported in some studies [6,27,28], also LF/HF ratio (the ratio of absolute power in low frequency and high frequency bands extracted from HRV through frequency domain analysis) can be considered a physiological indicator for human thermal comfort prediction. Liu et al. [6] found a difference in LF/HF ratio at comfort and discomfort levels, while Yao et al. [27] and Zhu et al. [28] observed a different LF/HF under different environments, with the air temperature which had the most significant effects on LF/HF [28] as visible in Figure 12.

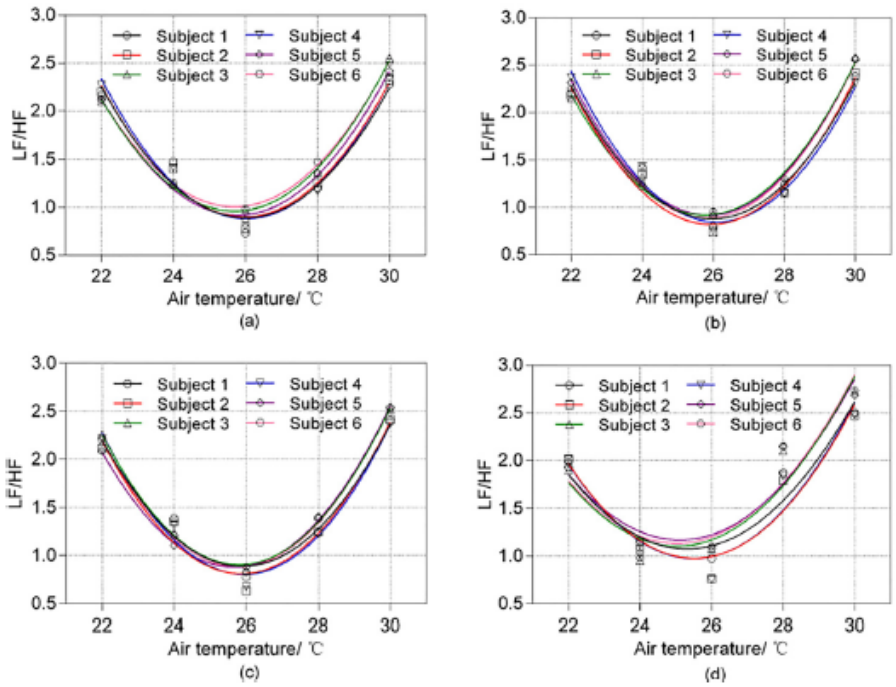

Figure 12. Changes of LF/HF under different air temperature. a: RH = 30%; b: RH= 45%; c: RH = 60%; d: RH = 80%) [28].

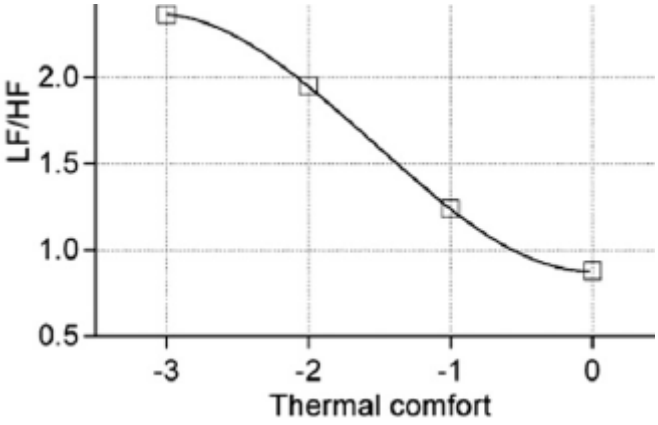

Figure 13. LF/HF relations with thermal comfort.

The relationships between LF/HF and thermal comfort (Figure 13) show that a higher LF/HF indicates thermal discomfort, while a low LF/HF indicates a thermally acceptable state. Furthermore, since LF peak is related to sympathetic and parasympathetic activity and HF peak infers the vagal activity, LH/HF ratio can be used to evaluate thermal comfort level.

Besides ECG, also electroencephalogram (EEG) is useful for thermal comfort prediction. It consists in recording brain waves (alpha, beta, delta, theta) through electrodes placed in specific positions on the scalp. The studies of Deboer et al. [29, 30] show that waves frequencies in the EEG change with the change of brain and body temperature, that affect also EEG power density spectra. Yao et al. [31] studied EEG signals and proved the possibility of predicting human thermal comfort through them. The results displayed that there was a close relationship between HRV, EEG, and human thermal comfort but in any case, HRV had more relevance. In another study, Yao et al. [27] investigated the impact of different indoor temperatures on EEG signal of subject and deduced that the power of several EEG frequency ranges was different under different temperatures. Choi et al. [32] used an 8 channels EEG headset to monitor brain activity in various indoor environment and determined that temporal lobe beta waves can be used to assess the thermal sensation. Shan et al. [33] analysed the strength of EEG-based methods to improve human-building interaction under several indoor temperatures, investigating the relationship between EEG and subjective perceptions and tasks. Their results showed that the EEG frontal asymmetrical activity was related to the subjective questionnaire and the objective tasks performance. Furthermore, their developed ML based model for EEG type

recognition demonstrated to be accurate in classifying the different mental states under different thermal conditions. Finally, Kanosue et al [34] found using functional magnetic resonance imaging (fMRI) that thermal signals from skin reach specific regions in the cerebral cortex, which means that thermal sensations can be reflected by EEG wave patterns.

Another consideration can be made after analysing the work of Chaudhuri et al. [35], which predicted three types of thermal sensations: uncomfortable coolness, comfortable and uncomfortable warmth. In their thermal comfort prediction model they included, in addition to the Fanger's factors, parameters like age, gender and outdoor effective temperature, reaching a prediction accuracy in air-conditioned buildings of 85.3% using artificial neural network (ANN), versus the 65.5% of the classic PMV model, and in naturally ventilated buildings of 73.14% using support vector machine (SVM) and logistic regression (LR), versus the 41.64% of the PMV model. So, from this study it emerges that age, gender and outdoor temperature, which are not included in the PMV model, are relevant factors for thermal comfort prediction.

From this research it emerges that thermal sensation of the occupant can be well reflected by specific physiological parameters, which can be monitored by dedicated body sensors:

- Electroencephalographic (EEG) sensors, which consist in electrodes placed on the scalp able to record the electrical activity of the brain;
- Electro-Dermal Activity (EDA) sensors, which monitor skin conductivity between electrodes placed on it (usually on wrist or on fingers);
- Heart Rate (HR) sensors, which measure and/or display HR in real time or record it for successive analysis. The most used in this area are the Electrocardiographs (ECG), able to measure the potential generated by electrical signals that control the expansion and contraction of heart chambers, and the Photoplethysmographic (PPG) ones, which instead use a light-based technology to measure the blood volume controlled by the pumping action of the heart;
- skin temperature sensors, which include infrared thermal cameras, thermistors and thermocouples, with these last two directly placed on the skin.

However, wearing sensors like electrodes for the acquisition of the ECG and EEG is an invasive procedure and is not reproducible in daily living environments. Fortunately, there are non-invasive wearable sensors able to register physiological parameters without relying on stationary infrastructure and without causing discomfort to the owner. Other

advantages include low cost, market penetration, ease of use and capability to monitor health. An example of these wearable sensors are chest belts monitors, fitness trackers and smartwatches, with the latter which today are almost part of daily living. These devices are gaining popularity because have reduced dimensions, so are comfortable to wear, and because they offer constant 24-hour monitoring of various physiological parameters. Most of them include a PPG sensor capable of extracting HRV, thus replacing the ECG, while others integrate also sensors capable of measuring skin temperature and blood pressure.

The PPG sensor's system is equipped with a light source (light emitting diodes) and a photodetector (Figure 14). The light traveling through tissues passes many materials, including arterial and venous blood. PPG sensor can optically detect changes in the blood flow volume due to changes in the detected light intensity in the microvascular bed of tissue through the reflection from or transmission through the tissue [36].

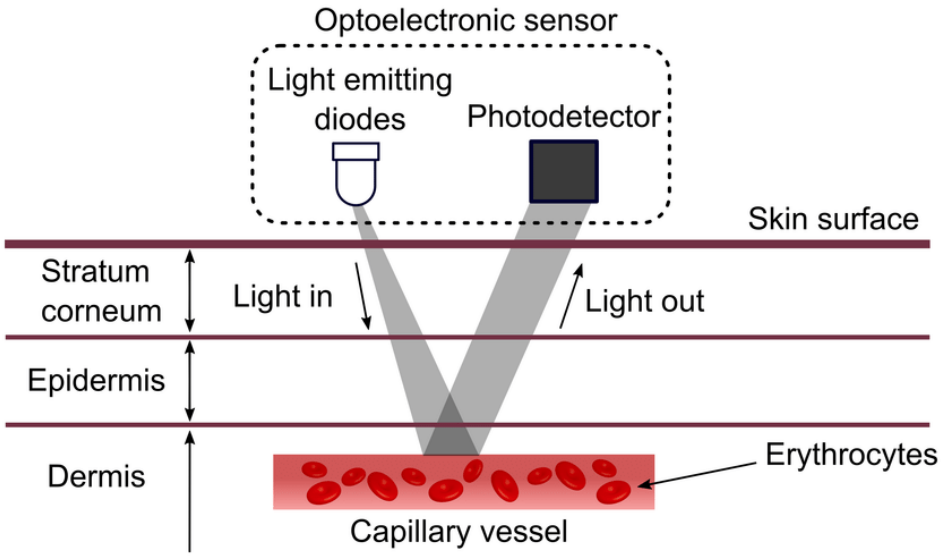

Figure 14. PPG sensor consisting of light emitting diodes and a photodetector. The emitted light travels through the tissues and is reflected towards the photodetector which measures its intensity. PPG can detect changes in the blood flow volume due to changes in the detected light intensity in the microvascular bed.

HRV signal from ECG is calculated from RR interval, while the HRV signal from PPG signal is extracted from inter-beat interval (IBI) [37]. Figure 15 shows both the ECG and PPG signals.

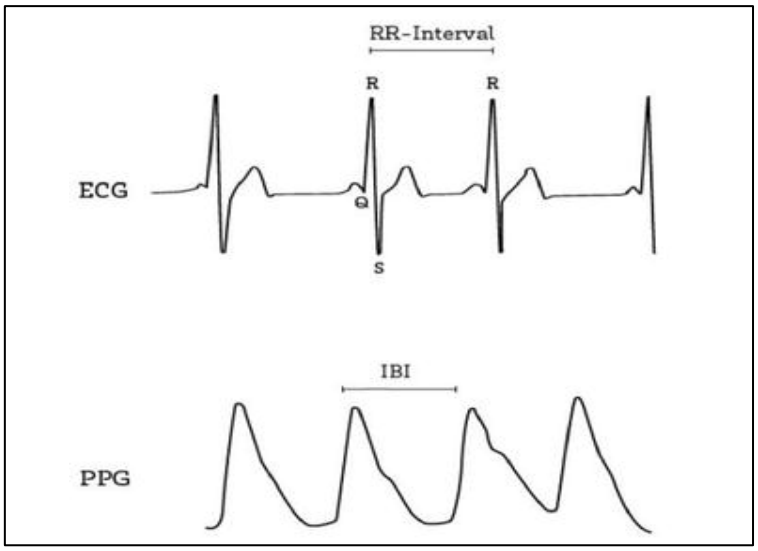

Figure 15. ECG and PPG signals.

Several factors must be considered to ensure the reliability of the acquired data. The position of the sensor on the body plays an important role as different areas give different readings accuracies. The most accurate are recorded in the earlobe, however the wrist allows readings with adequate accuracy [36]. An advantage of using watches equipped with PPG sensors is that they are not subject to electrical interference and drying or dropping of the electrodes. The review of Georgiou et al. [38] about wearable devices shows that especially those which use PPG sensors provide a good alternative solution for measuring HRV, but they are precise only at resting or mild exercise conditions, like those of paperwork, as their accuracy diminishes with increasing exercise load. Also, Tsoi et al. [39] showed that wearable devices are a reliable instrument for HRV measurement in static posture, recommending more investigations to assess the accuracy during motion. However, it is difficult to compare the accuracy of wearable devices with respective reference instruments in order to choose the more appropriate one. This was highlighted by Cosoli et al. [40] which, analysing the state of the art on the accuracy of wearable sensors, found a lack of a standard test protocol, population characteristics and metrological parameters to consider for the validation of these devices, highlighting the necessity of defining specific guidelines for the determination of the accuracy. The emerging sensing technology of these devices anyway gives the chance to apply the measured data to predict indoor thermal comfort.

Regarding the ML algorithm to use in the model, there are many typologies of them which can be used in this scenario, each one with a certain degree of accuracy. In their study

Zhao et al. [41] proposed an intelligent thermal comfort control system based on the Internet of Things (IoT) and artificial intelligence (AI). The PMV prediction model that they developed was based on a Back Propagation Neural Network (BPNN) and reached a high thermal comfort prediction accuracy, with moreover the capability of automatically completing a series of operations through IoT hardware devices placed at multiple locations in the building. Also, Yang et al. in their study [42] verified the feasibility of a thermal comfort prediction model with a BPNN. The model was based on the use of physiological parameters extracted from the ECG, blood pressure and EDA signals. They compared the model with the classical PMV one, finding an equivalent accuracy, meaning that using BPNN is a reasonable option for achieving a good prediction accuracy.
Other models used in this type of learning problem are the Support Vector Machine (SVM), a supervised learning model associated with learning algorithms for regression (Support Vector Regression (SVR)) and classification, the Random Forest (RF) and the Logistic Regression (LR). Each of these has been used by researchers to predict thermal comfort [12,13,26,35], obviously reporting different accuracy values that depend not only on the capabilities of the ML model itself, but also on the parameters considered and on the amount of data used in the learning phase of the model.

The analysis of the state of the art allowed to get an overview about the parameters to consider for the person's thermal comfort prediction in indoor environments. Considering all the analysed studies, in the proposed model it was chosen to include, also making a comparison (Figure 16) among all the possible sensors through which the parameters would be acquired, the classic Fanger's factors (PMV model) and the time and frequency domain features extracted from HRV, since their non-invasiveness and accuracy in predicting thermal comfort. The Fanger's factor relative to the environment, such as air temperature and relative humidity, could be acquired through specific sensors like hygrometers and thermometers. The HRV will be acquired through a smartwatch (Samsung Galaxy Watch) using the PPG sensor installed on it. As shown in Figure 16, the smartwatch has been selected for its non-invasiveness and its diffusion in daily use, for its relative low cost, and above all for the accuracy in extracting the HRV demonstrated in everyday life situations.

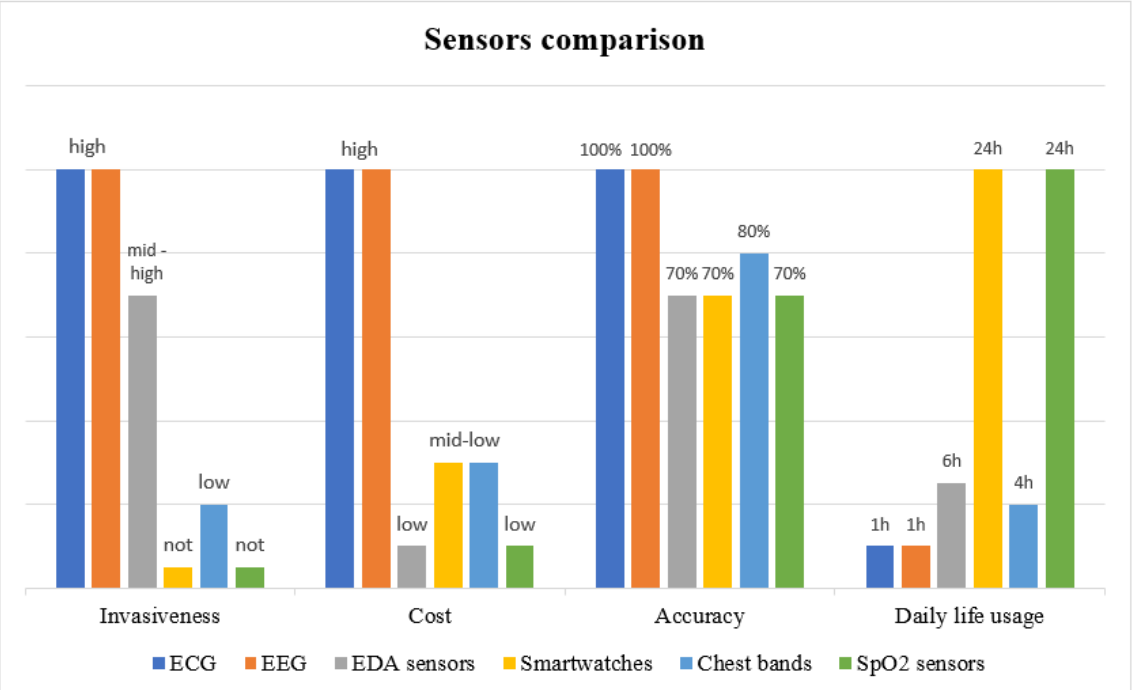

Figure 16. Sensors comparison: ECG, EEG, EDA sensors, smartwatches, chest bands and SpO_2 sensors are compared taking in consideration their invasiveness, cost, accuracy and daily life usage. ECG= Electrocardiograph; EEG= Electroencephalograph; EDA= Electro-Dermal Activity sensors; $SpO_{2=}$ Blood oxygen saturation sensors.

CHAPTER 3

MATERIALS AND METHODS

The aim of this project is to develop a real-time acquisition system from a sensors network, made of environmental and wearable devices, able to predict through a ML algorithm the occupant thermal comfort, and to compute the optimal ambient temperature accordingly. The sensors that make up the system capable of acquiring the parameters necessary for this purpose are listed in Table 1. The experimental setup for the real-time acquisition and processing of signals, schematized in Figure 18, was carried out inside a room of defined dimensions (Figure 19). The scheme is subdivided into four blocks which represent the main operations that the system performs: the acquisition of physiological parameters, the acquisition of the thermal sensation vote (TSV) of the occupant, the acquisition of environmental parameters and the processing of the acquired signals. The whole system is managed through a code developed in Python language that controls every procedure, from the signals acquisition to their processing passing through the creation of a communication network between the sensors and the processing unit. The acquisition of the physiological parameters was possible thanks to the use of a smartwatch, through which the HRV and the HR were acquired, while the subject's TSV was recorded through the use of a questionnaire, collected using a web page, to be used as ground truth for the training phase of the algorithm (Figure 17).

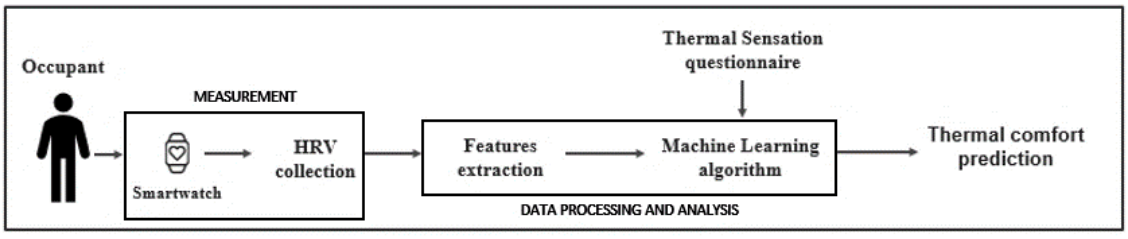

Figure 17. Block scheme for the analysis of the physiological quantities acquired with the smartwatch.

The acquisition of the environmental parameters was instead carried out using a sensor capable of measuring the air temperature (t_a) inside the room and its relative humidity (RH). The signals thus acquired were transmitted through different types of communication channels to the heart of the system: a computer that manages the whole

processing. In the development of the project, the Raspberry Pi 3 B+ was used as the data processing unit, which consist in a low-cost small computer. This device was chosen because of the advantage of allowing programming in different languages including Python, used in the development of the code underlying the operations of the system, and of being able to interface with the sensors useful for our purpose. After various operations, thanks to the use of the ML algorithm, the system was able to predict as output the value of the TSV of the subject within that specific environment and to propose the optimal temperature to be set.

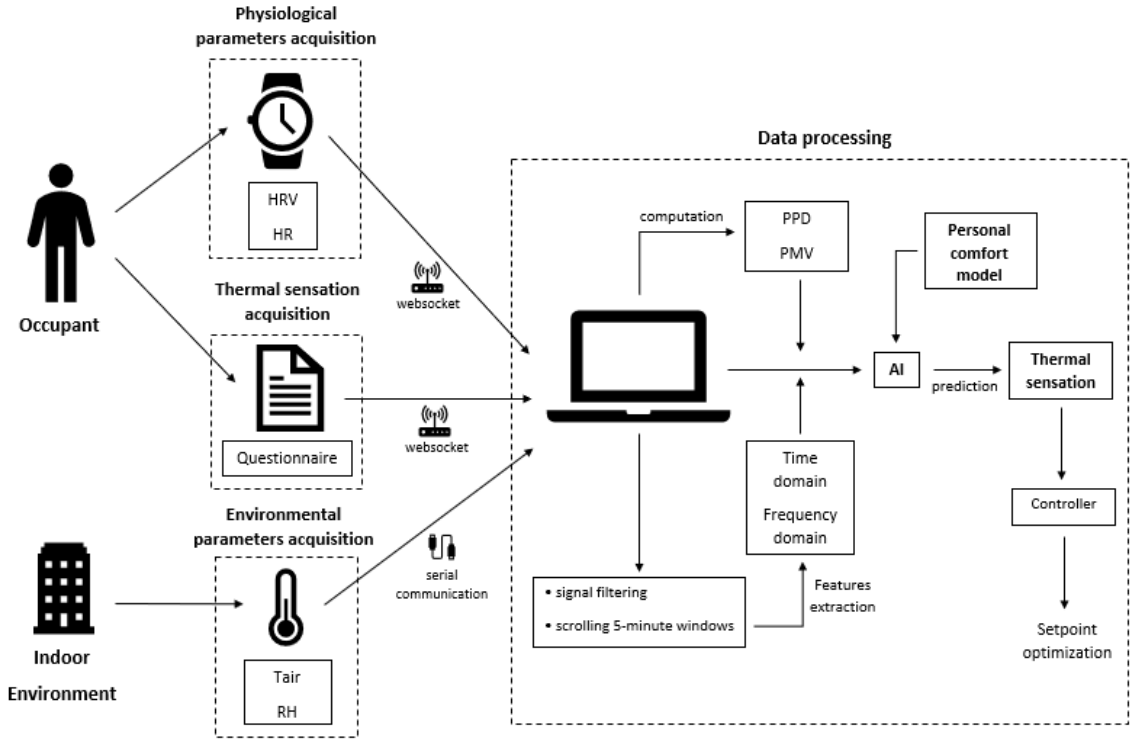

Figure 18. Scheme of the experimental setup.

Table 1. List of sensors and their specifics.

INSTRUMENTS	DESCRIPTION	RANGE	ACCURACY
SAMSUNG GALAXY WATCH	PPG sensor for HR and HRV monitoring	N/A	May diminish depending on measurement conditions and surroundings
DHT11	Air temperature sensor	0 – 50 °C	± 0.1 °C
DHT11	Relative humidity sensor	20 – 90 %	± 0.1 %

3.1 Experimental setup

The tests were conducted in a room with dimensions of 4.8 m (length) × 2.9 m (width) × 3.0 m (height) inside the DIISM (Dipartimento di Ingegneria Industriale e Scienze Matematiche) of the Università Politecnica delle Marche. The room planimetry is visible in Figure 19, while its three-dimensional reconstruction in Figure 20 shows the internal layout, where we can see the workstation equipped with a PC where the test was carried out. The test consisted of monitoring a series of subjects during office work. In the room during the test were present the participant to it and a second one in charge of positioning the sensors and controlling the cooling and heating systems. Before entering the room, the subjects were made aware of the methods of conducting the experiment. At this point, they entered in the room and wore the sensor necessary for the measurement of physiological parameters. Subsequently they were subjected to a period of acclimatization, after which there was a lowering of the room temperature using a portable air conditioner and then its increase through an electric heater, in order to create thermal discomfort. The test had a duration which varies from 40 minutes to 1.30 hours and six subjects participated. During the test, each one placed a vote ranging from -3 (cold) to +3 (hot) on the web page questionnaire for each variation of his/her thermal sensation. The data collected during the test were HR, HRV, air temperature and relative humidity.

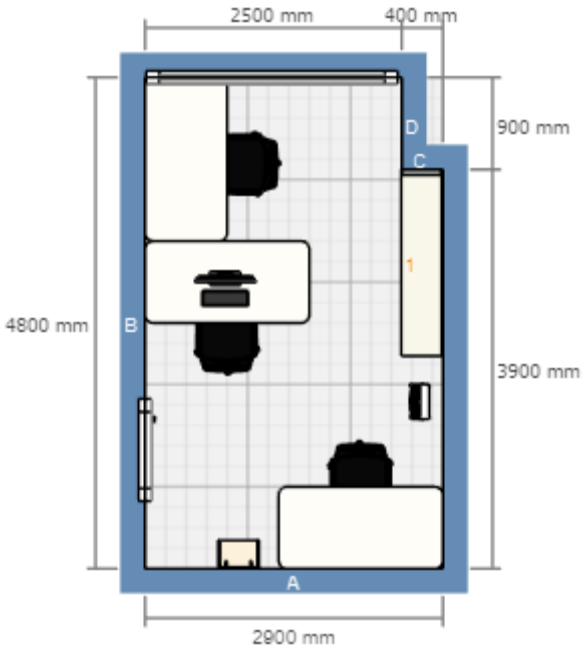

Figure 19. Two-dimensional planimetry with attached dimensions of the test room.

Figure 20. Three-dimensional plan of the test office.

3.2 Physiological parameters acquisition

As previously mentioned, the acquisition of the occupant's physiological signals was carried out thanks to the use of a smartwatch: the Samsung Galaxy Watch. Being equipped with a PPG sensor, it can analyse the vital parameters of the wearer in a non-invasive way, measuring his HR and HRV.
The following describes the sensor and the acquisition and communication method for signals storage.

3.2.1 Samsung Galaxy Watch

The Samsung Galaxy Watch was selected in this study for collecting occupants' biometric data. It is a mid-range wearable device with Tizen operating system in 4.0 version which houses an advanced heart monitoring system that can help to improve habits. The smartwatch is equipped with a PPG sensor capable of extracting the heartbeat from changes in the skin's light absorption. Once you have found the HR and HRV it is necessary to collect them. To do this, a dedicated application was developed through Tizen Studio, a software that provides a complete set of tools for developing Linux-based mobile applications. The application in question, called "getHRV" (Figure 21), once started, can work in background for extracting HR and HRV signals from the smartwatch and sending them in real-time via a WebSocket communication to the Raspberry.

Figure 21. Samsung Galaxy Watch in which the "getHRV" application is installed.

The data transmission has been set to 1 sample per second to make the acquisition real-time, as shown below in the application code block in Figure 22.

```
// SET INTERVAL OF COMMUNICATION
var myCallbackInterval = 1000;
var mySampleInterval = 1000;
var option = {
                'callbackInterval': myCallbackInterval,
                'sampleInterval': mySampleInterval
            };
```

data transmission set to 1000 ms

Figure 22. Extract of the JavaScript code for the transmission of HR and HRV signals from the smartwatch every second.

The WebSocket communication protocol (Figure 24) is an advanced technology that opens an interactive communication session between a server (the Raspberry) and a client (the smartwatch). To make this possible, the smartwatch and the Raspberry must be connected to the same local network (LAN) so that, knowing the Raspberry IP address and the communication port, they are able to establish a secure connection and subsequently provide for the transmission of the data (Figure 23).

```
// START WEBSOCKET
var webSocketUrl = 'ws://192.168.0.102:8085';
var webSocket = new WebSocket(webSocketUrl);
webSocket.onopen = function(e) {
      console.log ('CONNECTED, readyState: ' + e.target.readyState);
};
webSocket.onerror = function(e) {
      console.log ('NOT CONNECTED, readyState: ' + e.target.readyState);
};
```

IP

data port

Figure 23. Extract of the JavaScript code from the "getHRV" application for the connection request of the smartwatch to the Raspberry.

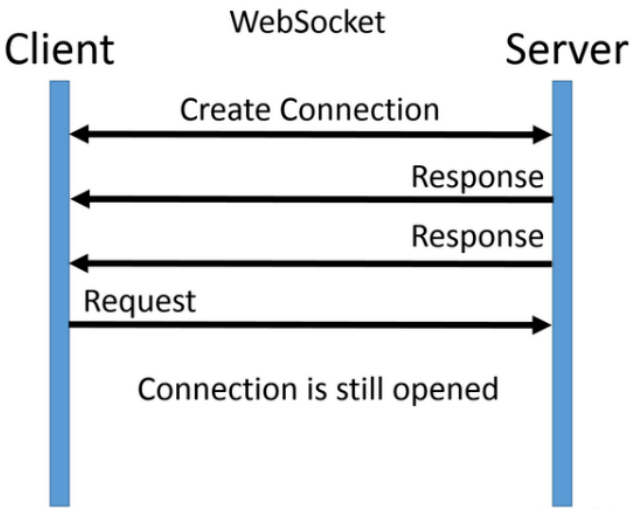

Figure 24. WebSocket communication protocol between client and server.

3.3 Thermal sensation vote acquisition

The acquisition of the subject's thermal sensation vote (TSV) inside the room was carried out thanks to the use of a questionnaire developed as a web page (Figure 25). Since the test consists in simulating a normal office working condition, it was decided to develop the questionnaire as a web page in such a way that anyone, while working on the PC, is able to access it and place the own vote whenever his/her thermal sensation changes. The vote is then used as ground truth for training the prediction algorithm.

The questionnaire was developed in HTML language, setting up a window in which the participant enters the name and a series of buttons each correspondent to a value of the thermal scale of the perceived sensation. During the test therefore, the subject can express an opinion on his/her own thermal sensation with a vote from -3 to +3 belonging to the ASHRAE's thermal scale. The vote will then be sent via a WebSocket connection to the Raspberry. As long as the participant, after having carried out a vote, does not carry out a subsequent one when his thermal comfort state changes, the system will ensure that the previous vote is maintained for the entire duration of this time period of transition. In this way, the web page will acquire the subject's vote and will send this 1 time per second to the Raspberry, to ensure time synchronization with the rest of the acquired data.

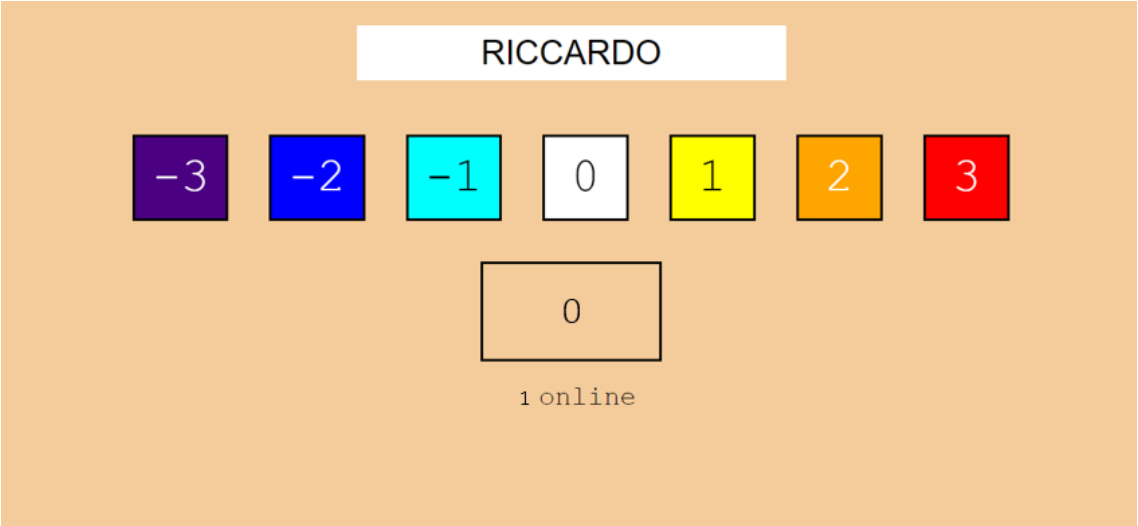

Figure 25. Web questionnaire in which the subject enters his name in the appropriate window and expresses his opinion through a series of buttons corresponding to the ASHRAE's thermal scale.

3.4 Environmental parameters acquisition

This paragraph describes how to acquire the environmental parameters and the sensors used. The t_a and RH were acquired through a single sensor capable of simultaneously measuring the two quantities, while as regards the air speed (v_a) and the mean radiant temperature (MRT), a separate discussion must be made. Given that in a working environment such as an office the possibility of a large displacement of air in a short time is very low, it was decided to set a v_a value of 0.1 m/s, considered an assumable value in heat transfer calculations. Regarding the MRT Meghan et al. [43] evaluated the difference it has with respect to the t_a in conditioned office buildings. They based their findings on measurements from 48 offices from the ASHRAE's Global Thermal Comfort Database [44] and on laboratory experiments [45]. In the first case they found a difference of just 0.4 °C between MRT and t_a, while in the second case they observed that MRT was 0.3 °C higher respect the air one. From this it is clear that measuring the t_a of an environment in typical conditions is sufficient to estimate the MRT, therefore it is not necessary to install sensors for its measurement since the two can be assumed equal. That said, in the present work it has considered that the MRT of the room was equal to that of the air.

3.4.1 Air temperature and relative humidity sensor

The DHT11 is a commonly used temperature and humidity sensor. It comes with a dedicated thermistor to measure temperature and an 8-bit microcontroller to output the values of temperature and humidity as serial data. The sensor is also factory calibrated and hence easy to interface with other microcontrollers. It can measure temperature from 0 °C to 50 °C and humidity from 20% to 90% with an accuracy of ±1 °C and ±1 %, respectively [46].

The sensor implements a 1-wire protocol, in other words it allows to communicate the detected values to the Raspberry using a single wire in addition to the power and ground wires. This feature is very important as the Raspberry is not equipped with analog pins and therefore it is not immediately possible to use sensors of this type. First of all it is therefore necessary to connect the sensor to the Raspberry using the cables that start from the 3 pins of the sensor: one for the power supply (VCC) which needs a voltage between 3 V and 5 V, one for the grounding (GND) and one for data transmission (SIG). As shown in Figure 26, each of these cables starts from a sensor pin and is connected to a specific pin of the Raspberry according to the task to be performed.

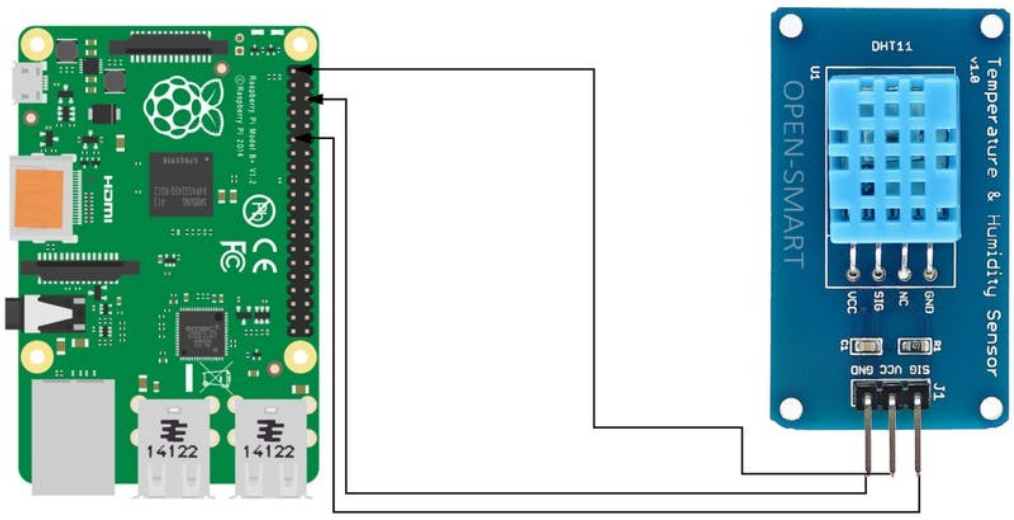

Figure 26. DHT11 sensor (on the right) connected through 3 cables which start from ground pin (GND), signal pin (SIG) and voltage one (VCC) to end in the respective pins on the Raspberry (on the left).

To use the sensor with the Raspberry it is necessary to use the Adafruit_DHT library, through which it is possible to write the code block in Python (Figure 27) for the acquisition of the temperature and humidity signals.

```
import Adafruit_DHT
DHT11 = Adafruit_DHT.DHT11
DHT11_PIN = 21
while True:
    humidity, temperature = Adafruit_DHT.read_retry (DHT11, DHT11_PIN,
retries=2, delay_seconds=1)
    if humidity is not None and temperature is not None:
        print('Temperature={0:0.1f}*C
Humidity={1:0.1f}%'.format(temperature, humidity))
    else:
        print ('Acquisition Error!')
```

Figure 27. Extract of the Python code for the acquisition of the temperature and humidity signals.

3.5 Data processing

Once all the necessary signals have been acquired through the sensor setup, the amount of data was stored and processed in real-time following a well-determined procedure which is subsequently explained step by step.

3.5.1 Data filtering

The first operation to be carried out when receiving the signals from the sensors is the filtering and the removal of the outliers [47]. As for the environmental signals this was not necessary, or rather the data were acquired unless the sensor was able to perform the measurement. Another matter is what concerns the filtering of cardiac signals acquired by the smartwatch. In this context, a filtering was performed to remove any outlier and/or ectopic beat by creating specific functions in Python language, shown below. The first function ("remove_outliers") replaces the RR intervals not comprised in the specified range (400 – 1200 ms) with the previous RR value, while the second one ("remove_ectopic_beats") removes the ectopic beats if present through the "is_ectopic"

function, set to find the RR intervals differing by more than the 25% from the ones proceeding them, also in this case substituting them with the previous RR value.

- Function for the outliers' removal:

```
def remove_outliers (rr_intervals: List[float], verbose: bool = True,
low_rri: int = 400, high_rri: int = 1200) -> list:
    rr_intervals_cleaned = [rri if high_rri >= rri >= low_rri else
rri-1 for rri in rr_intervals]
    if verbose:
        outliers_list = []
        for rri in rr_intervals:
            if high_rri >= rri >= low_rri:
                pass
            else:
                outliers_list.append(rri)
       count = count + 1
       if count == 0:
         print("{} outlier(s) have been deleted.".format(count))
       else:
         print("{} outlier(s) have been deleted.".format(count))
         print("The outlier(s) value(s) are:{}".format(outliers_list))
    return rr_intervals_cleaned
```

- Function for the ectopic beats' removal:

```
def remove_ectopic_beats (rr_intervals: List[float],
custom_removing_rule: float = 0.2, verbose: bool = True) -> list:
    outlier_count = 0
    previous_outlier = False
    nn_intervals = [rr_intervals[0]]
    for i, rr_interval in enumerate(rr_intervals[:-1]):
        if previous_outlier:
            nn_intervals.append(rr_intervals[i + 1])
            previous_outlier = False
            continue
```

```
        if is_ectopic(rr_interval, rr_intervals[i+1],
custom_rule=custom_removing_rule):
                nn_intervals.append(rr_intervals[i + 1])
        else:
            nn_intervals.append(rr_intervals[i])
            outlier_count += 1
            previous_outlier = True
    if verbose:
       print("{} ectopic beat(s) have been
deleted.".format(outlier_count))
    return nn_intervals
```

- Function for the detection of ectopic beats:

```
def is_ectopic (rr_interval: int, next_rr_interval: float,custom_rule:
float = 0.2) -> bool:
   ectopic = abs(rr_interval - next_rr_interval) <= 0.25 * rr_interval
    return ectopic
```

3.5.2 Data windowing

At the basis of the procedure useful for extracting the parameters necessary for predicting thermal comfort is the archiving of the acquired signals. Since the system was designed to work in real-time, each data was acquired with a frequency of 1 sample per second. The processing begins 5 minutes after the start of the "getHRV" application on the smartwatch, a time that is considered enough for the subject's thermal acclimatization in the environment. The trigger of the entire system is therefore given by the start of the application, after which each sensor sends its signal to the Raspberry, which stores them inside lists. At this point, the creation of windows containing the acquired signals lasting 5 minutes each takes place [47]. Over time, each window is shifted by 1 sample (corresponding to 1 second of acquisition) with respect to the previous one. From these windows, the parameters (listed in Table 2) used as input for the prediction algorithm are computed. In particular, each physiological parameter is calculated for each 5-minute window, while the environmental parameters are processed by calculating the average over each window of the environmental signals themselves.

Table 2. Parameters used in the prediction algorithm computed from each 5-minute signal window.

PHYSIOLOGICAL PARAMETERS		ENVIRONMENTAL PARAMETERS
Frequency domain features	**Time domain features**	PMV
LF	MEAN	PPD
HF	MEDIAN	Relative Humidity
LF/HF	RMSSD	Air Temperature
HF/LF	SDANN	
VLF		
TP		

3.5.3 PMV/PPD computation

Taking up the Fanger's model already explained in the paragraph 1.3.1, in the calculation of the PMV and PPD indices are used as inputs the air temperature, the relative humidity, the mean radiant temperature, the air velocity, the insulation of the clothes and the metabolic rate. While the first four parameters have been acquired or imposed in the modality already described, the clothing insulation and the metabolic rate are variables which depend from subject to subject. Since the test was carried out in the last week of September, the participants were wearing trousers and long-sleeved shirts, so a value of 0.6 clo corresponding to this clothing was set. The metabolic rate was set too at a specific value, which is of 1.1 met, matching the sedentary office work.

3.5.4 Time and Frequency parameters extraction

As explained in paragraphs 1.7.1 and 1.7.2, the parameters derived from HRV in the time and frequency domains are very useful for the prediction of thermal comfort. Their calculation was performed considering each 5-minute HRV window in order to obtain the parameters listed in Table 2 for each of them. Once extracted these were used as input for the prediction algorithm, so that a thermal sensation value for each window was obtained. Below are some graphs that have been obtained from HRV values taken as samples from

the entire amount of data acquired. Figure 28 represents the temporal trend of the RR intervals within a 5-minute window (corresponding to 300s), while Figure 29 shows RR intervals temporal distribution. Figure 30 shows the Poincaré plot between one NN interval and the next and Figure 31 the FFT spectrum, so the frequency components (VLF, LF and HF) of a window.

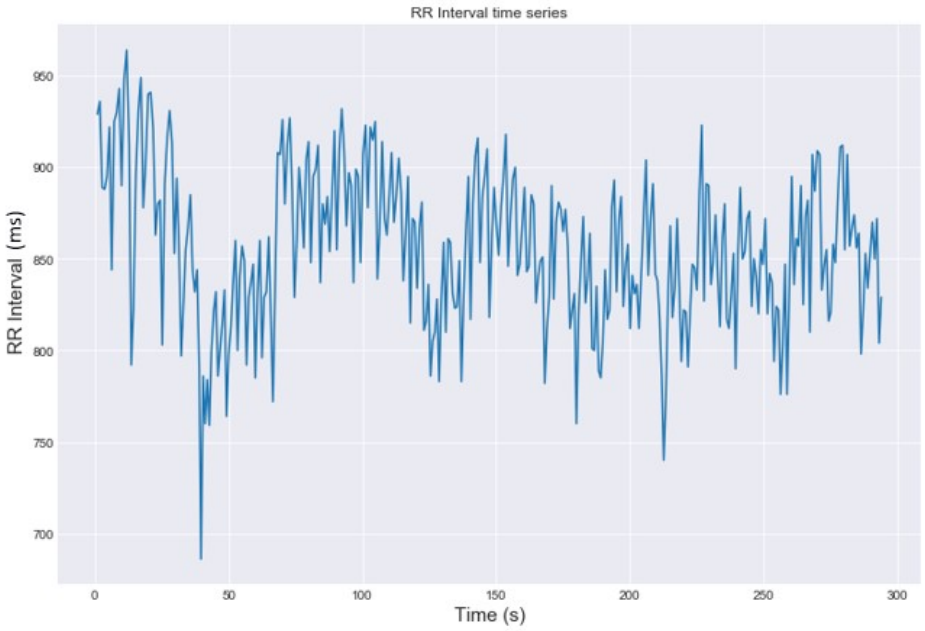

Figure 28. RR interval time series.

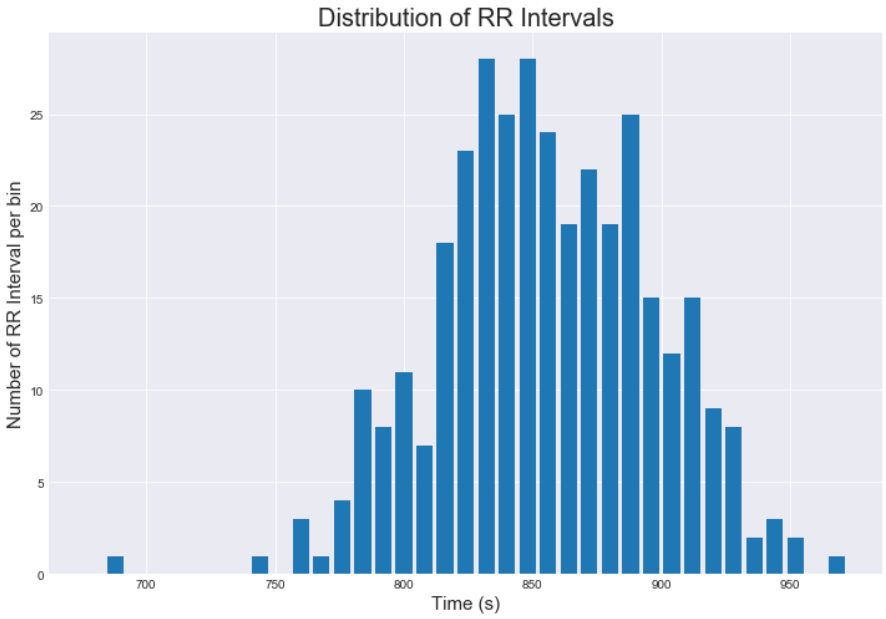

Figure 29. RR intervals time distribution.

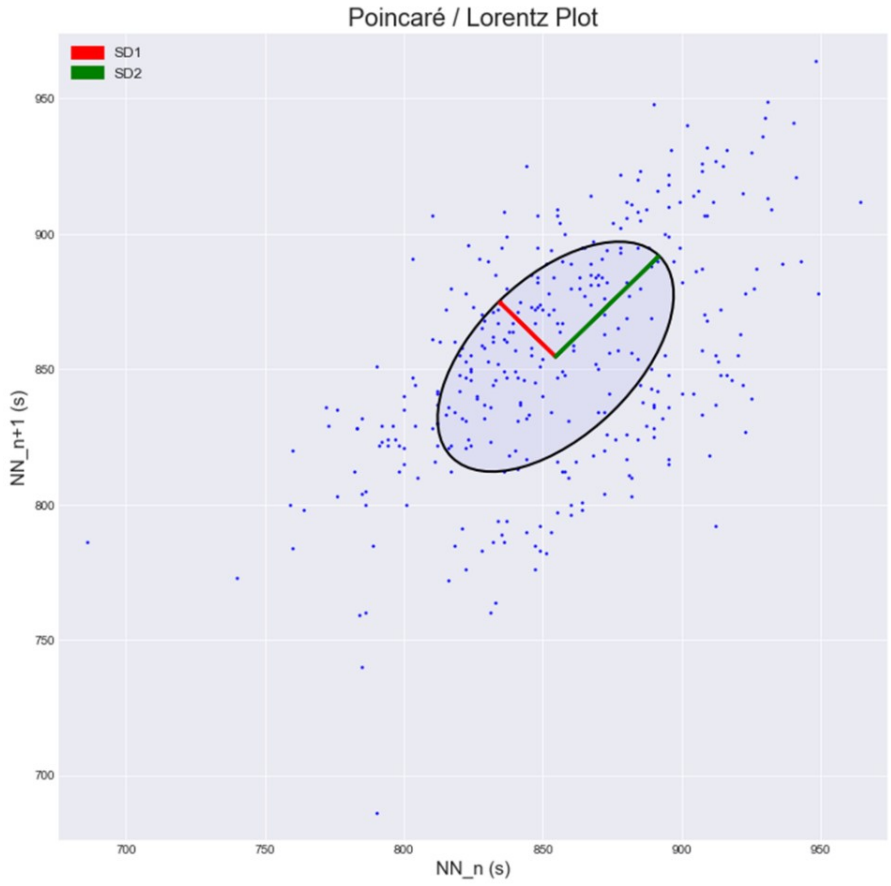

Figure 30. Poincaré plot.

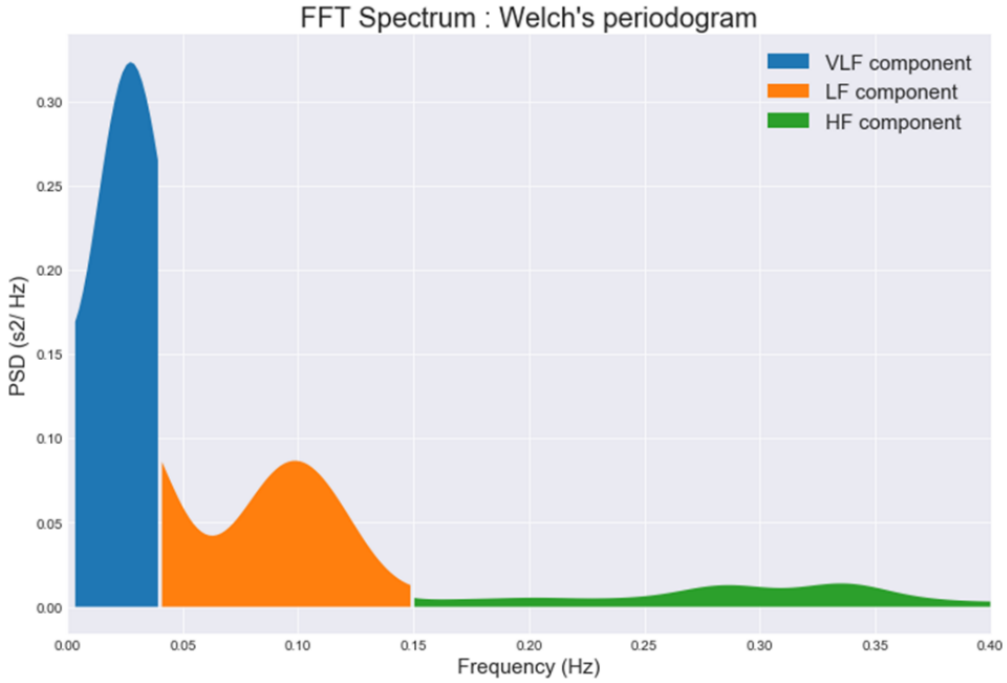

Figure 31. FFT spectrum. VLF = very low frequency; LF = low frequency; HF = high frequency.

3.5.5 Thermal comfort prediction algorithm choice

To develop an algorithm capable of predicting the sensation of thermal comfort of the occupant of an indoor environment, the three ML algorithms that in literature were found to be the most used in this area were compared:

- *Random Forest (RF):* method for classification, regression and other tasks that operate by creating a multitude of decision trees at training time and outputting the class that is the mode of the classes (classification) or mean prediction (regression) of the individual trees [13, 26, 48].
- *Logistic Regression (LR):* mathematical model used to estimate the probability of an event occurring having been given some previous data [35].
- *Support Vector Regression (SVR):* supervised learning algorithm for classification and regression analysis that trains using a symmetrical loss function, which penalizes high and low wrong values equally [49, 50].

These algorithms were tested on a pre-existing dataset relating to a study born from the collaboration of UNIVPM with the University of Perugia on thermal comfort. The dataset consists of 20 subjects whose physiological and environmental parameters acquired during the tests are reported, among which we find the same typologies used in this study (listed in Table 2). In this way it was possible to train each of the algorithms on the dataset to choose the best one. The training and testing of the algorithms was done using the LOSO (leave-one-subject-out) technique which consists in carrying out the training phase on the data of 19 of the 20 subjects iteratively, and the testing phase on the remaining subject. This procedure was repeated by changing the subject used for the test to evaluate the capabilities of the algorithms on different people. To assess their effectiveness, reference was made to the MAE and MAPE indices calculated in the test phase. MAE is a measure of the errors between the predicted and observed value of the same phenomenon. It is calculated through (5) as the arithmetic average of the absolute errors (e_i) between predicted (y_i) and actual (x_i) values.

$$MAE = \frac{\sum_{i=1}^{n} |y_i - x_i|}{n} = \frac{\sum_{i=1}^{n} |e_i|}{n} \quad (5)$$

MAPE is a measure of prediction accuracy of a forecasting method used for regression problems in ML. It expresses the accuracy through the formula:

$$MAPE = \frac{1}{n}\sum_{i=1}^{n} \left| \frac{x_i - y_i}{x_i} \right| \times 100\%, \quad (6)$$

where x_i is the actual value and y_i is the predicted one. The difference between x_i and y_i is divided by x_i and the absolute value of this computation is summed for every predicted point and then divided by the number of fitted points n. Multiplying by 100% it becomes a percentage error.

Therefore, to evaluate the accuracy of the algorithms, reference was made to the resulting MAE and MAPE values. As shown in Figure 32, the forecasting power is acceptable for MAPE values below 50%, becoming good for values between 10% and 20%, and very accurate for values smaller than 10% [51].

MAPE	Forecasting power
<10%	Highly accurate forecasting
10%~20%	Good forecasting
20%~50%	Reasonable forecasting
>50%	Weak and inaccurate forecasting

Source: Lewis (1982)

Figure 32. Forecasting power referred to MAPE values.

3.5.6 Personal thermal comfort model

After choosing the algorithm that was able to predict thermal sensation with greater accuracy, this was used in the creation of a personal thermal comfort model of the occupant. To do this, two tests were repeated for each subject who took part in the study. The first test consisted in varying the temperature of the room, first lowering and then raising it, in order to create discomfort in the occupant. During the test, the thermal sensation that the subject experienced was recorded through the questionnaire, which was then used in post-processing as ground truth in training the prediction algorithm. At this point, after having created a personal prediction model for each of the subjects, this was used in the second test, which, like the previous one, consisted in the variation of the ambient temperature for the generation of thermal discomfort. At the end, the ability of the personal algorithm to predict the thermal sensation was evaluated.

3.5.7 Indoor temperature optimization

Parallel to the real-time prediction of the thermal comfort of the person inside the room, the computation of the optimal air temperature takes place. The calculation is carried out by the system based on the predicted thermal sensation of the occupant, to ensure that it remains close to 0, i.e. in comfort. Ranges of predicted thermal sensation values have been established to match a variation in the actual temperature. The recommended temperature is in fact the same as the actual one to which a value is subtracted or added to guarantee the permanence of thermal well-being. The temperature values of decrease or increase are shown in Table 3 in relation to the respective predicted range of thermal sensation.

Table 3. Predicted thermal sensation ranges and respective optimal indoor temperatures. The optimal temperature (T_{opt}) is computed as the actual one (T_{act}) to which is summed or subtracted a value corresponding to the predicted sensation (TSV) in order to keep it in the comfort range.

PREDICTED THERMAL SENSATION VOTE	OPTIMAL INDOOR TEMPERATURE
$TSV > 2.5$	$T_{opt} = T_{act} - 2$ °C
$1.5 < TSV \leq 2.5$	$T_{opt} = T_{act} - 1.5$ °C
$0.5 < TSV \leq 1.5$	$T_{opt} = T_{act} - 1$ °C
$-0.5 \leq TSV \leq 0.5$	$T_{opt} = T_{act}$
$-0.5 > TSV \geq -1.5$	$T_{opt} = T_{act} + 1$ °C
$-1.5 > TSV \geq -2.5$	$T_{opt} = T_{act} + 1.5$ °C
$TSV < -2.5$	$T_{opt} = T_{act} + 2$ °C

CHAPTER 4

EXPERIMENTAL RESULTS

4.1 Machine learning algorithm selection

Table 4 shows the MAE and MAPE values related to the test phase of the three compared algorithms (SVR, LR, RF) carried out on each of the 20 subjects present in the dataset. To choose the most accurate algorithm, the average of MAE and MAPE values (reported at the bottom of Table 4) was computed. Figure 33 represents a comparison between the results of the test phase of the three ML algorithms on some subjects taken as example.

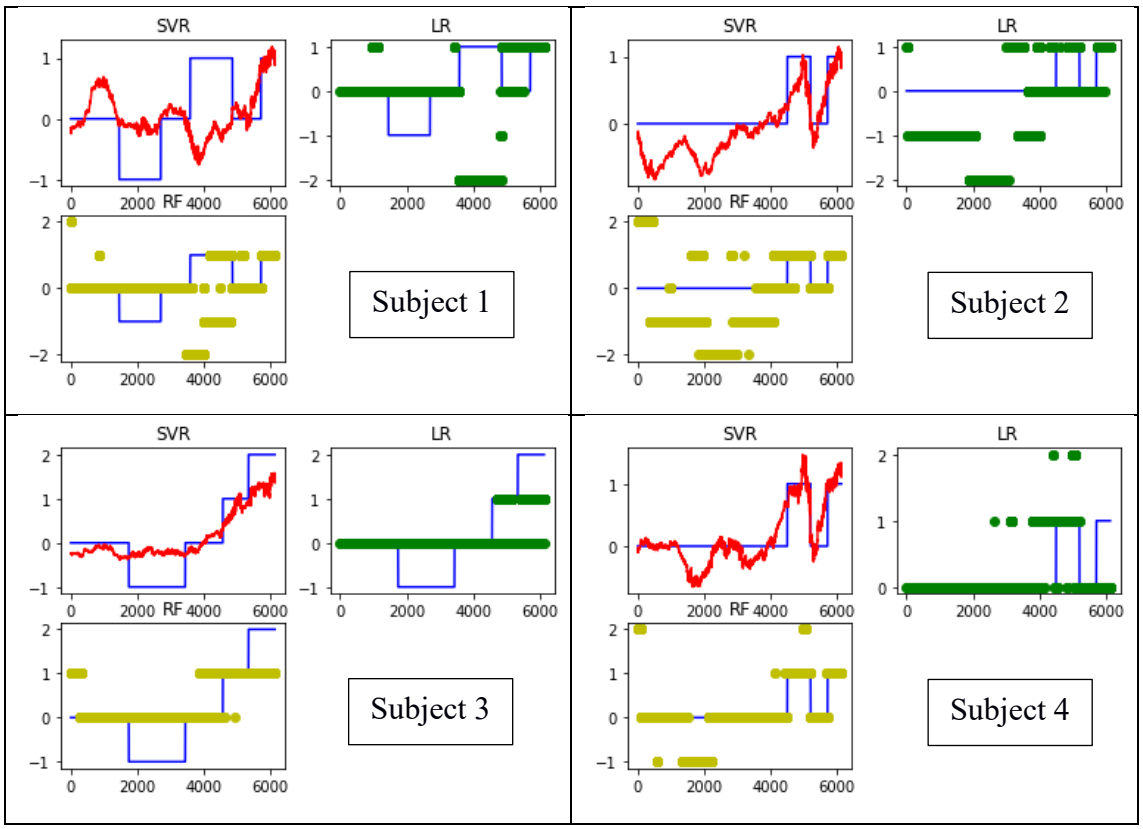

Figure 33. Comparison of SVR (red line), LR (green line) and RF (yellow line) algorithms' prediction results on subjects 1 (top left), 2 (top right), 3 (bottom left) and 4 (bottom right). In each graph are reported on the x axis the data samples and on the y axis the predicted thermal sensation vote. The blue line represents the real thermal sensation vote acquired through questionnaire.

Table 4. MAE and MAPE calculated between true and predicted TSVs of SVR, LR and RF algorithms for each of the 20 subjects that make up the database.

	MAE			**MAPE** [%]		
Subject	**SVR**	**LR**	**RF**	**SVR**	**LR**	**RF**
1	0.53	0.92	0.56	16.10	22.35	18.06
2	0.34	0.88	0.88	12.17	23.87	26.29
3	0.43	0.54	0.52	18.12	21.50	22.04
4	0.20	0.19	0.16	10.39	7.24	10.41
5	0.43	0.92	0.56	13.69	16.80	18.04
6	0.35	0.67	0.74	12.05	20.42	21.34
7	0.40	0.54	0.50	14.01	17.23	18.76
8	0.33	0.57	0.53	13.52	21.35	19.69
9	0.37	0.28	0.70	10.83	9.80	16.05
10	0.76	1.02	0.99	34.27	44.89	47.30
11	0.40	1.54	1.44	15.11	31.17	32.55
12	0.44	0.28	0.30	14.22	13.89	14.99
13	0.40	1.11	0.41	10.52	28.27	10.36
14	0.56	0.59	0.40	11.33	11.71	10.36
15	0.60	1.37	0.43	14.82	31.31	10.34
16	0.46	0.43	0.41	11.41	10.38	10.72
17	0.34	0.42	0.51	9.44	11.26	13.45
18	0.56	0.71	0.63	23.54	34.10	28.90
19	0.60	0.83	0.74	31.40	40.58	37.20
20	0.42	0.38	0.61	17.64	15.23	18.75
Average	**0.44**	**0.70**	**0.60**	**15.70**	**21.67**	**20.28**

Figure 34 shows four examples of test results of the SVR algorithm on subject 5 (top left), 6 (top right), 8 (bottom left) and 9 (bottom right).

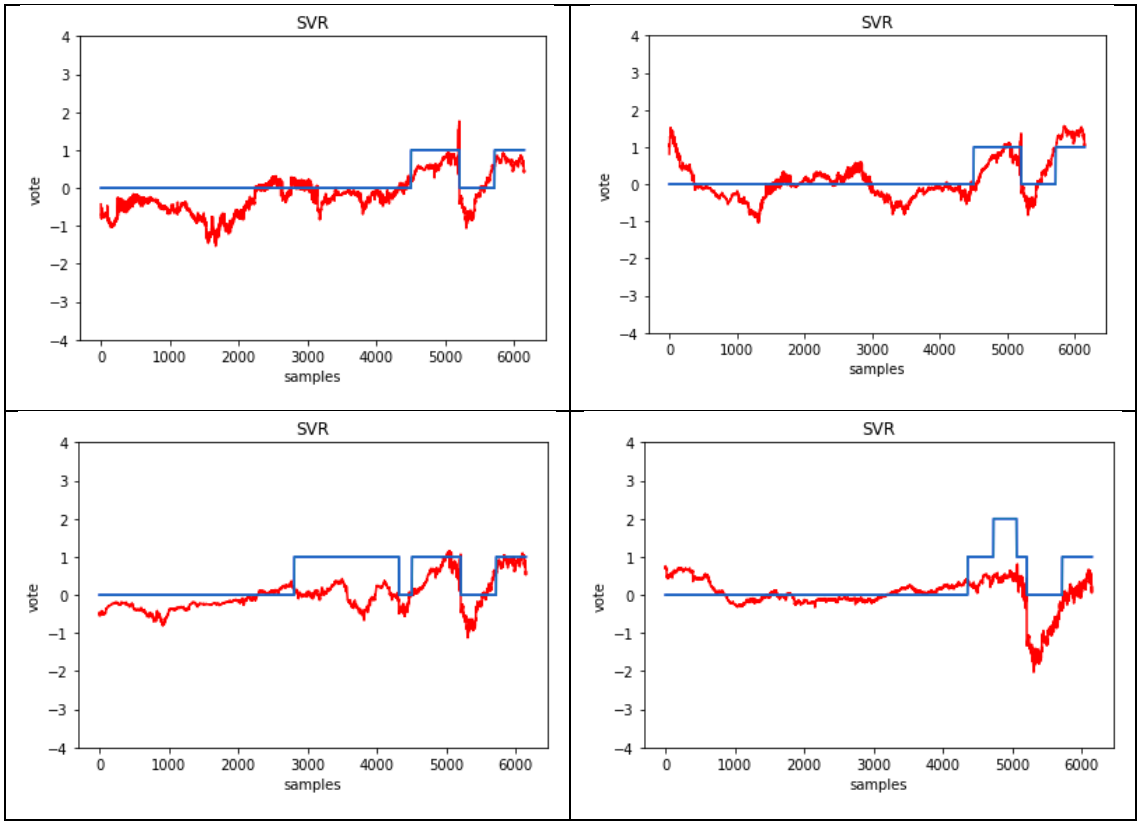

Figure 34. Representation of SVR algorithm test results on subject 5 (top left), 6 (top right), 8 (bottom left) and 9 (bottom right). The red line indicates the predicted thermal sensation vote while the blue line represents the real vote acquired through questionnaire.

4.2 Thermal comfort prediction results

In this paragraph the results related to the prediction of the TSV of each of the 6 individuals who took part in the tests are reported.

For each subject in Figure 35, the blue stars refer to LF/HF values extracted from the HRV signal. For each temperature value, the average of LF/HF (represented by the red triangle) was calculated. The average values thus found were linked together (red line) in order to show the trend of LF/HF with respect to air temperature.

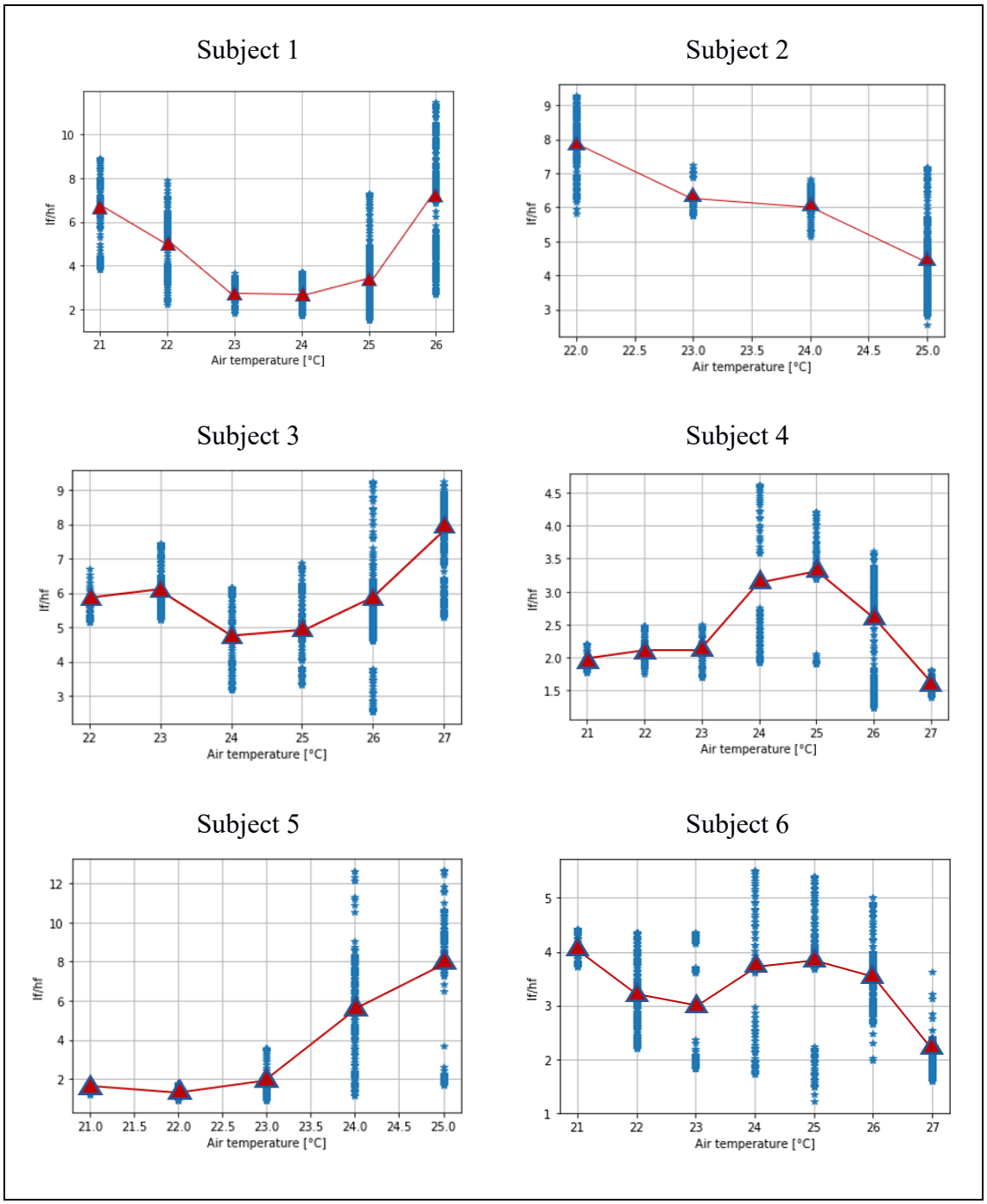

Figure 35. LF/HF trend (red line) with respect to air temperature of the 6 subjects. The blue stars refer to each LF/HF value extracted from the HRV signal. The red triangles represent the average values of LF/HF for each air temperature.

Table 5 lists the MAE and MAPE values of the subjects who participated in the test. To evaluate the effectiveness of the prediction algorithm, the average MAE and MAPE were calculated and reported in Table 5.

Table 5. MAE and MAPE values of the tested subjects and their average.

Subject	MAE	MAPE [%]
1	0.32	8.92
2	0.35	10.57
3	0.45	11.21
4	0.52	15.78
5	0.46	12.46
6	0.54	14.33
Average	0.44	12.21

4.2.1 Subject 1

Subject 1 was a 27-year-old man who was subjected to a test lasting approximately 90 minutes. Figure 36 shows the filtered HRV signal recorded by the smartwatch during the test, as well as Figure 37 shows the HR signal.

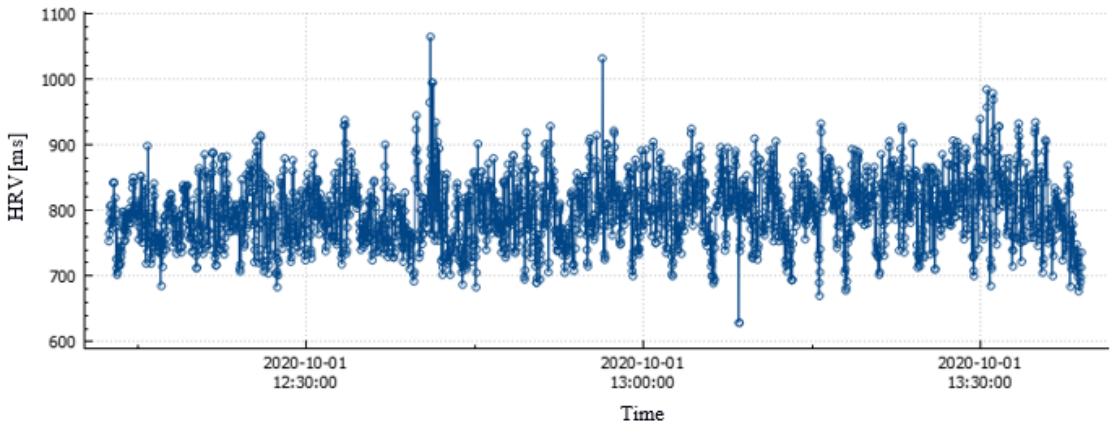

Figure 36. HRV signal recorded by the smartwatch during the test.

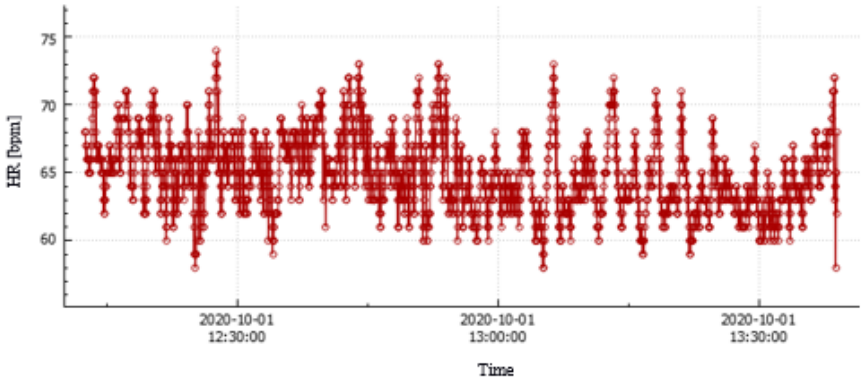

Figure 37. HR signal recorded by the smartwatch during the test.

Figure 38 shows at the top the real TSV compared to the predicted one with the relative MAE and MAPE values, at the bottom instead the LF/HF ratio compared to the real TSV (left) and the air temperature (right).

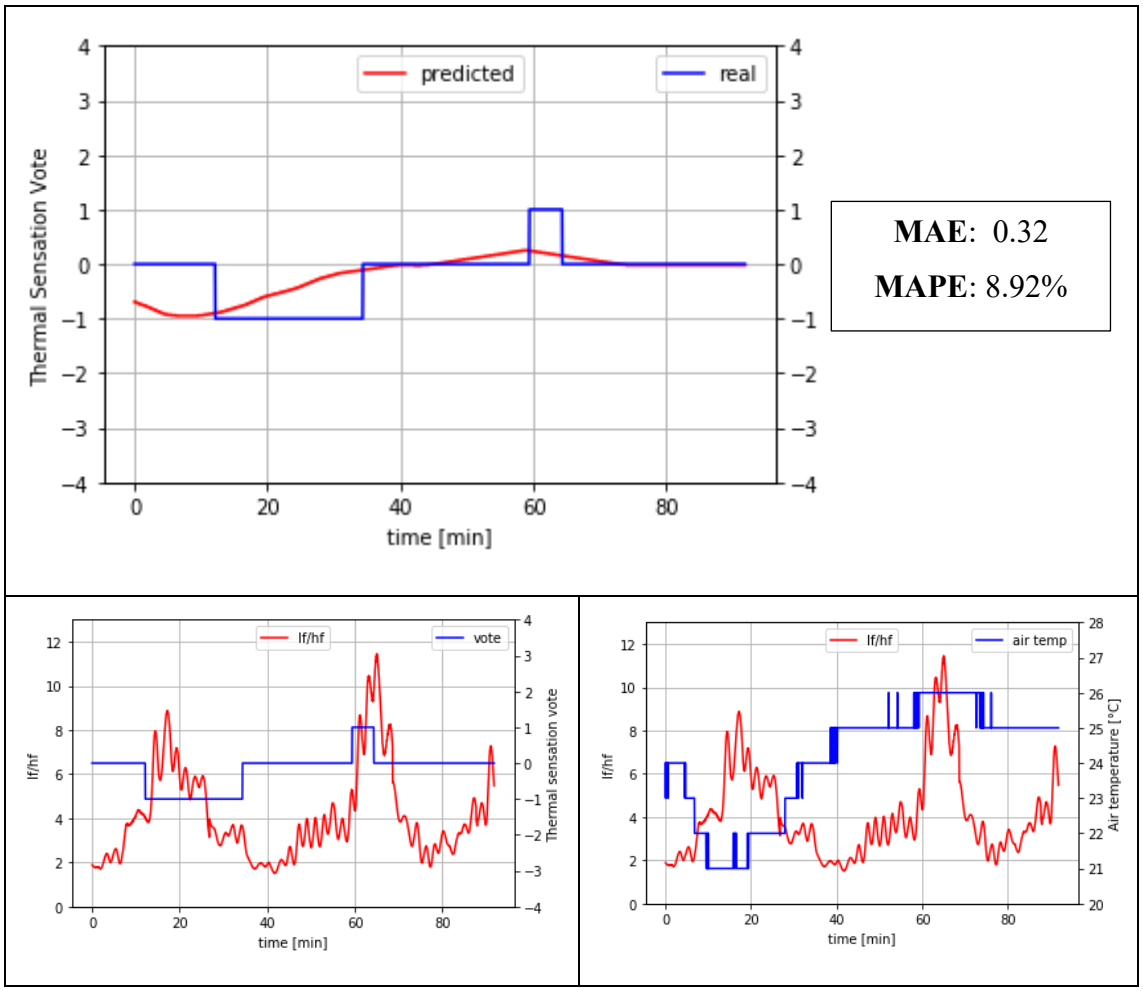

Figure 38. At the top is represented the occupant's TSV registered during the test (blue line) and the respective predicted value (red line) by the algorithm, both reported in relation to the test duration. On the side are reported the MAE and MAPE values calculated between the predicted

thermal sensation votes and the real ones. At the bottom left are represented the LF/HF values (red line) and the TSV (blue line) for the duration of the test. At the bottom right, the LF/HF values (red line) and the air temperature in the room (blue line) during the test are displayed.

4.2.2 Subject 2

Subject 2 was a 23-year-old woman who was subjected to a test lasting 50 minutes. Figure 39 shows at the top the real TSV compared to the predicted one with the relative MAE and MAPE values, at the bottom instead the LF/HF ratio compared to the real TSV (left) and the air temperature (right).

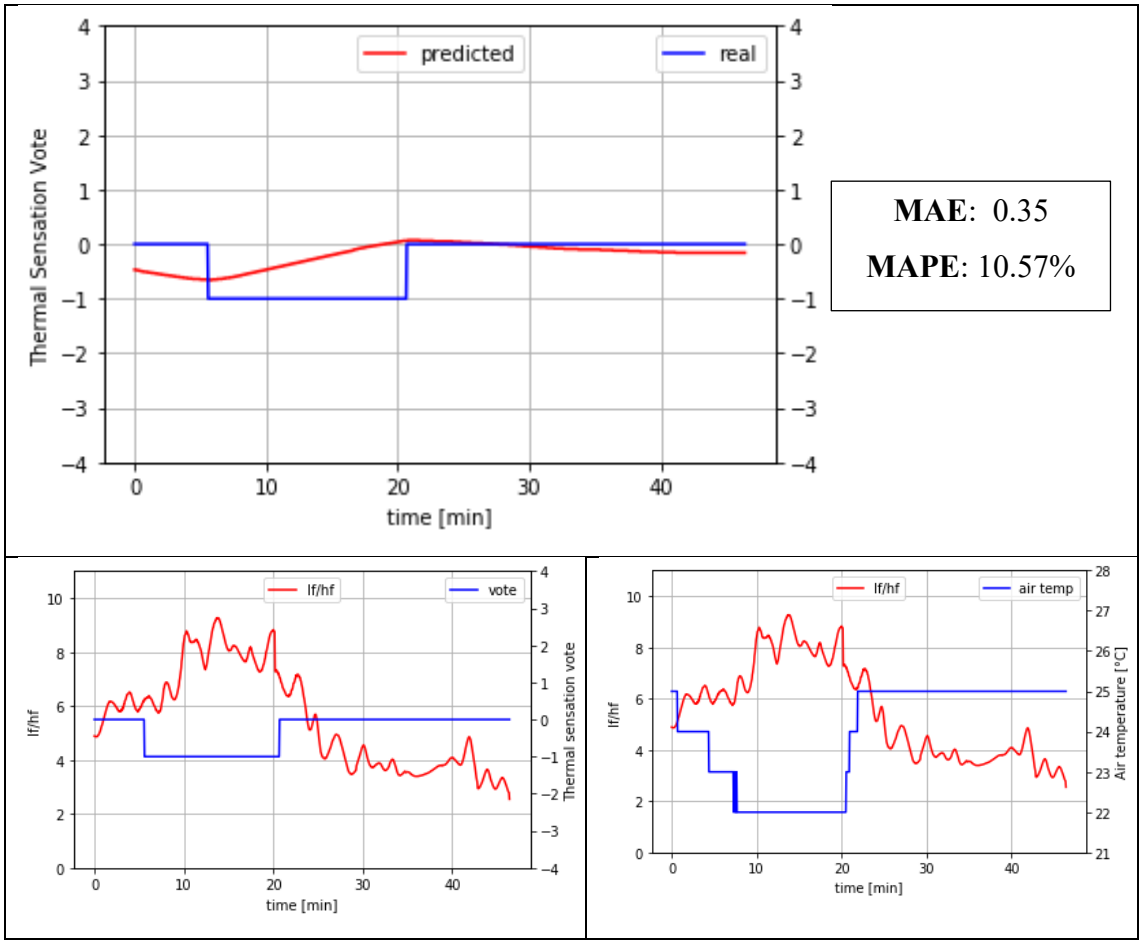

Figure 39. At the top is represented the occupant's TSV registered during the test (blue line) and the respective predicted value (red line) by the algorithm, both reported in relation to the test duration. On the side are reported the MAE and MAPE values calculated between the predicted thermal sensation votes and the real ones. At the bottom left are represented the LF/HF values (red line) and the TSV (blue line) for the duration of the test. At the bottom right, the LF/HF values (red line) and the air temperature in the room (blue line) during the test are displayed.

4.2.3 Subject 3

Subject 3 was a 29-year-old man who was subjected to a test lasting 45 minutes. Figure 40 shows at the top the real TSV compared to the predicted one with the relative MAE and MAPE values, at the bottom instead the LF/HF ratio compared to the real TSV (left) and the air temperature (right).

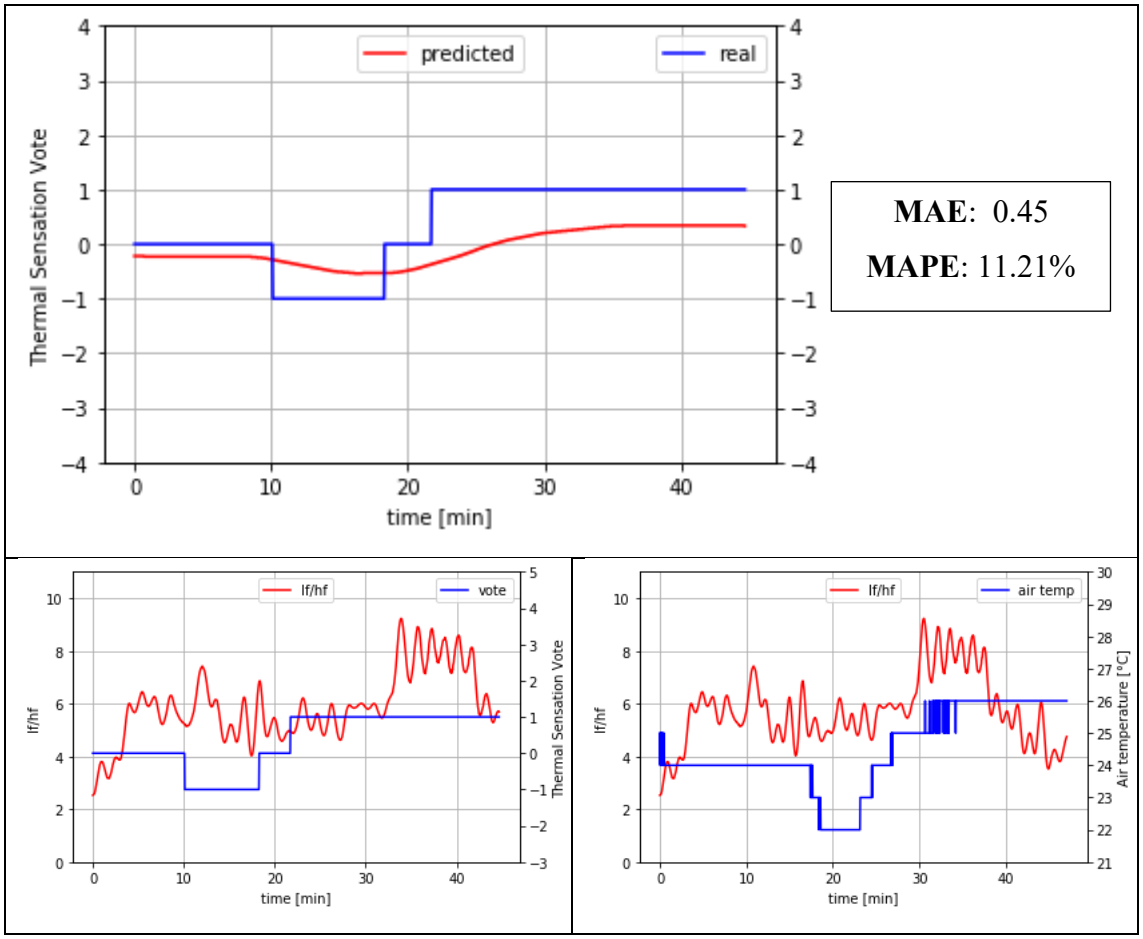

Figure 40. At the top is represented the occupant's TSV registered during the test (blue line) and the respective predicted value (red line) by the algorithm, both reported in relation to the test duration. On the side are reported the MAE and MAPE values calculated between the predicted thermal sensation votes and the real ones. At the bottom left are represented the LF/HF values (red line) and the TSV (blue line) for the duration of the test. At the bottom right, the LF/HF values (red line) and the air temperature in the room (blue line) during the test are displayed.

4.2.4 Subject 4

Subject 4 was a 26-year-old man who was subjected to a test lasting approximately 55 minutes. Figure 41 shows at the top the real TSV compared to the predicted one with the relative MAE and MAPE values, at the bottom instead the LF/HF ratio compared to the real TSV (left) and the air temperature (right).

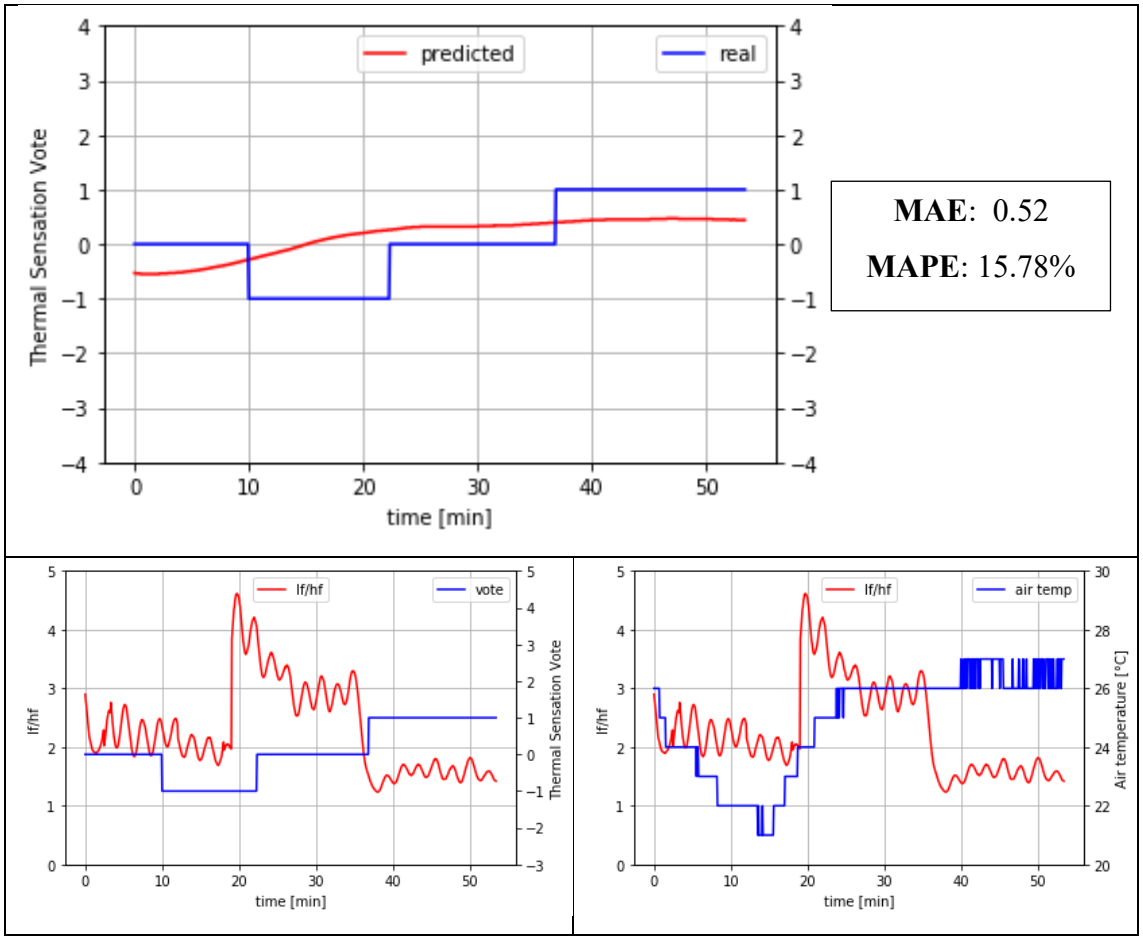

Figure 41. At the top is represented the occupant's TSV registered during the test (blue line) and the respective predicted value (red line) by the algorithm, both reported in relation to the test duration. On the side are reported the MAE and MAPE values calculated between the predicted thermal sensation votes and the real ones. At the bottom left are represented the LF/HF values (red line) and the TSV (blue line) for the duration of the test. At the bottom right, the LF/HF values (red line) and the air temperature in the room (blue line) during the test are displayed.

4.2.5 Subject 5

Subject 5 was a 23-year-old man who was subjected to a test lasting 75 minutes. Figure 42 shows at the top the real TSV compared to the predicted one with the relative MAE and MAPE values, at the bottom instead the LF/HF ratio compared to the real thermal sensation vote (left) and the air temperature (right).

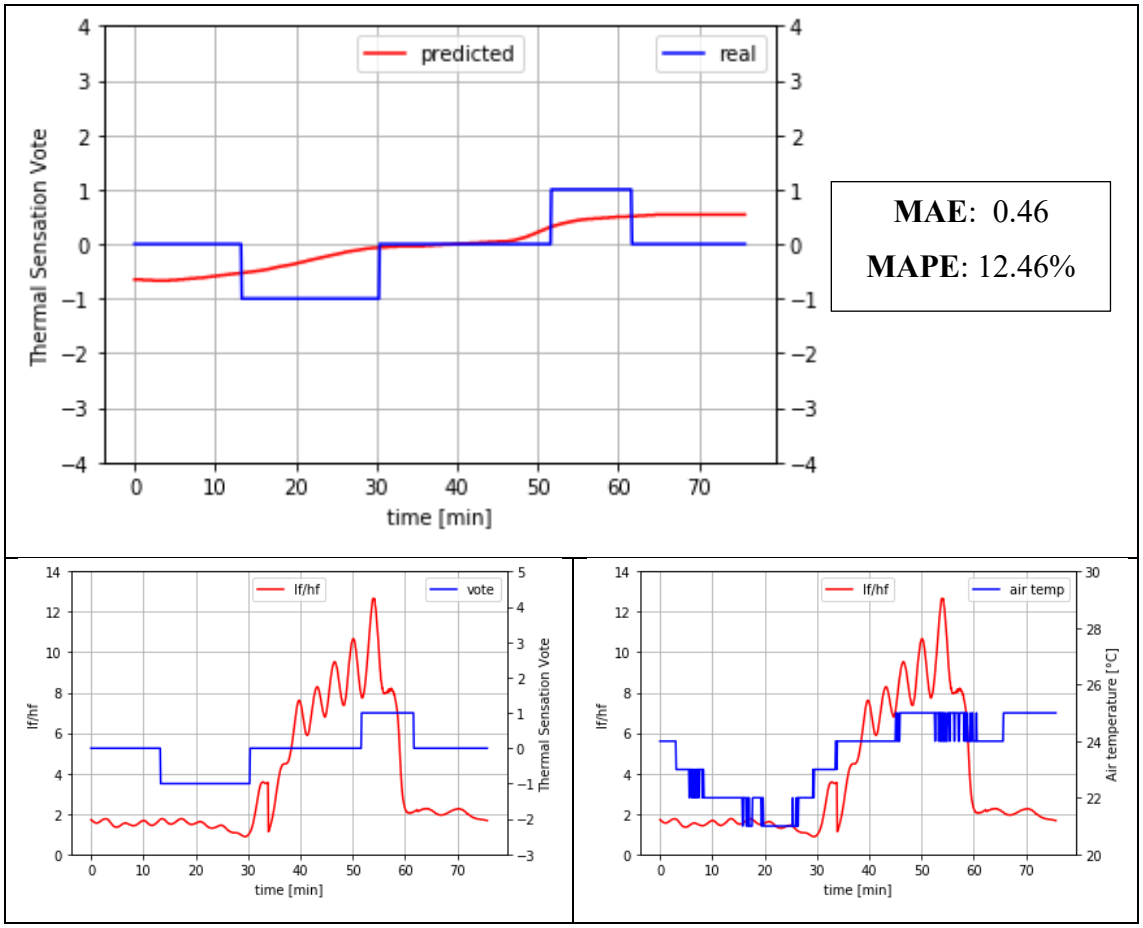

Figure 42. At the top is represented the occupant's TSV registered during the test (blue line) and the respective predicted value (red line) by the algorithm, both reported in relation to the test duration. On the side are reported the MAE and MAPE values calculated between the predicted thermal sensation votes and the real ones. At the bottom left are represented the LF/HF values (red line) and the TSV (blue line) for the duration of the test. At the bottom right, the LF/HF values (red line) and the air temperature in the room (blue line) during the test are displayed.

4.2.6 Subject 6

Subject 6 was a 19-year-old woman who was subjected to a test lasting approximately 65 minutes. Figure 43 shows at the top the real TSV compared to the predicted one with the relative MAE and MAPE values, at the bottom instead the LF/HF ratio compared to the real thermal sensation vote (left) and the air temperature (right).

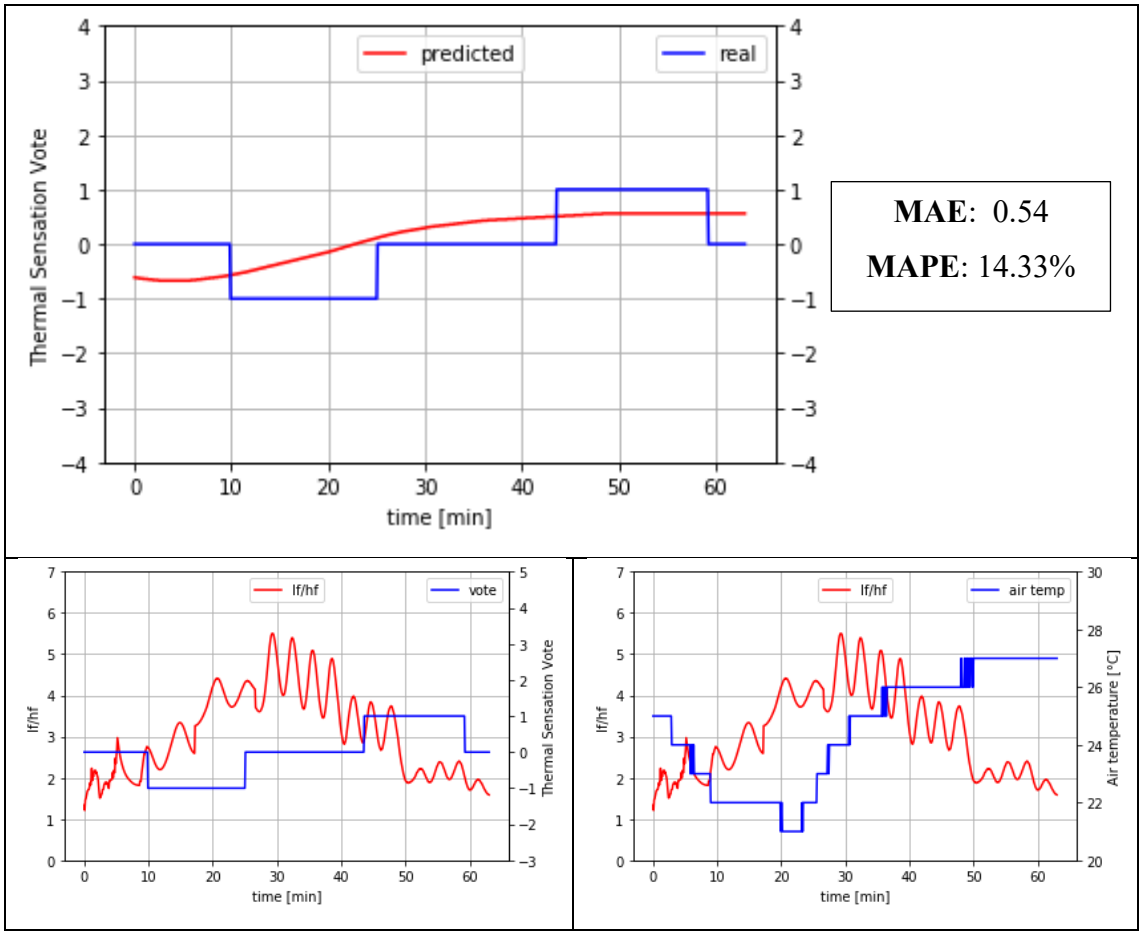

Figure 43. At the top is represented the occupant's TSV registered during the test (blue line) and the respective predicted value (red line) by the algorithm, both reported in relation to the test duration. On the side are reported the MAE and MAPE values calculated between the predicted thermal sensation votes and the real ones. At the bottom left are represented the LF/HF values (red line) and the TSV (blue line) for the duration of the test. At the bottom right, the LF/HF values (red line) and the air temperature in the room (blue line) during the test are displayed.

CHAPTER 5

DISCUSSIONS AND CONCLUSIONS

The aim of the project was to build a sensors system capable of acquiring physiological and environmental signals in real time and processing them so that the extracted parameters could be used as input for an algorithm that predicted the occupant's TSV within the environment. The first step, which consisted in the development of the signals acquisition and processing system through the creation of a communication network between sensors, has been successfully completed. The following step consisted in choosing the ML algorithm to be used in the development of the predictive model of personal thermal comfort, which fell on SVR. Table 4 shows the values obtained for MAE and MAPE after testing each of the three algorithms (SVR, LR, RF), which the literature showed to be the most used in this field, on the subjects belonging to the dataset. Calculating the average values of MAE and MAPE for each algorithm, it turned out that the best one was SVR, which reported an average MAE of 0.44, against 0.70 for LR and 0.60 for RF, and an average MAPE of 15.70% against 21.67% of LR and 20.28% of RF. Referring to Figure 32, given the obtained average MAPE value of SVR, it was possible to state its good predictive power.

Once the algorithm with the highest prediction accuracy was identified, it was used in the creation of the personal thermal comfort prediction model. SVR is an algorithm typically used in regression analysis (i.e. it works with continuous data) which offers the use of different kernels (functions used to map a lower dimensional data into a higher dimensional data). In the present project the polynomial kernel was used since compared to those available (linear, polynomial, RBF, sigmoidal) it guaranteed a better prediction performance. The parameters taken as input for the algorithm (shown in Table 2) were the physiological ones, extracted from the HRV signal through time and frequency domain analysis, and the environmental ones, acquired by the DHT11 sensor and calculated using the Fanger's model.

The time course of the predicted and real thermal sensation values is shown in Figures 38 – 43, respectively in red and blue. For each of the subjects who took part in the test, Table 5 shows the MAE and MAPE values of the prediction of the thermal sensation with respect to the real vote. It can be observed that the average MAPE value among the

subjects is 12.21%, which means that the algorithm was able to predict the sensation of the occupant with good accuracy, while the resulting MAE value implies that on average the forecast's distance from the true value is 0.44.

The LF/HF ratio was analysed as the literature showed that its variation may reflect the thermoregulation of the person into an environment. In fact, it has been seen that the LF/HF in discomfort situations was higher than the one at a comfort level. When the ambient temperature changed during the test, each participant adapted to the new environment in a certain interval of time, which varied from subject to subject, manifesting discomfort situations, identified by the growth of the LF/HF signal, due to sensations of hot or cold. The increase in LF/HF reflects that nervous system activity has been increased to keep body heat in the normal range. In Figures 38, 39, 40 and 43 it is clearly visible that with a decrease in temperature the LF/HF of subjects 1, 2, 3 and 6 respectively, increases. If, on the other hand, we analyse the LF/HF in response to the rise in temperature, we notice that it increases for all subjects, for some during the temperature rising phase (subjects 2, 4, 5 and 6 in Figures 39, 41, 42, 43), for others after the maximum temperature has been reached (subjects 1, 3 in Figures 38, 40).

Given the literature, an increase in LF/HF was expected in response to temperature changes that created discomfort for the person. Referring to the TSV acquired through the web questionnaire, it is noted that not all subjects have an increase in LF/HF associated with declared thermal discomfort. While for subjects 1, 2, 3 and 6 it is evident from Figures 38, 39, 40 and 43, an increase in LF/HF compared to the vote carried out which reflects situations of discomfort (TSV equal to -1 or +1 in these cases), for subjects 4 and 5 the increased LF/HF is not associated with a declared discomfort situation (Figures 41, 42). This is due to a different response to temperature changes of each person during the test; probably there were those who voted for minimal changes in their state of well-being and those who had a greater ability to adapt to the new environment not feeling the need to change their TSV. Obviously, the subjective factor affecting the vote must be considered. Although participants were brought to an initial state of comfort through acclimatization prior to the test, mental or physical stressful situations may have developed during the test in response to different environmental situations. This must be taken into account in the analysis of the prediction results of the person's sensation of thermal comfort. In addition, other limitations can be considered the presence of possible artefacts due to sudden movements of the arm on which the smartwatch was worn during

the test, which may have affected the quality of the physiological data obtained, and the exposure to the sun of the room in which the tests have been carried out. This last factor affected the cooling phase of the room, which was in fact more complicated to perform than the heating phase, which was much faster as it was facilitated by exposure to the sun. All these factors may have limited the accuracy achieved by the thermal comfort prediction system.

The work presented proposes an innovative solution for the real-time measurement of thermal comfort of the person within an environment. Future developments will see the replacement of the Raspberry Pi 3 B+ with the more powerful Pi 4 version in order to increase the computational capabilities of acquisition and signal processing. Moreover, there will be the implementation in the system of a sensor for the skin temperature acquisition from the individual, which from literature appears to be a parameter capable of improving the prediction of TSV. A thermographic camera will be then inserted in the sensors network to measure the person's skin temperature in a non-invasive way. After its integration, it is planned to create a database on data acquired by people subjected to the same test methodology described in Paragraph 3.1, in order to have a substantial amount of data to be able to train the prediction algorithm to create a general model of thermal comfort prediction. The last step will consist in the implementation of an IoT thermostat that, from the output obtained from the system about the recommended ambient temperature, is able to set it automatically.

REFERENCES

[1] ANSI/ASHRAE standard 55, “Thermal environmental conditions for human occupancy”, *American Society of Heating*, *Refrigeration and Air-Conditioning Engineers*, 2013.

[2] P. O. Fanger, “Thermal Comfort: Analysis and Applications In Environmental Engineering”, *Copenhagen: Danish Technical Press*, 1970.

[3] R. de Dear, G. Brager, D. Cooper, “Developing an Adaptive Model of Thermal Comfort and Preference”, *Final Report ASHRAE RP-884, American Society of Heating, Refrigerating and Air Conditioning Engineers*, 1997.

[4] ISO 7730, “Moderate thermal environment-determination of the PMV and PPD indices and specification of the conditions for thermal comfort”, *International Organization for Standardization*, 2005.

[5] BS EN 15251, “Indoor environmental input parameters for design and assessment of energy performance of buildings addressing indoor air quality, thermal environment, lighting and acoustics”, *European Committee for Standardization*, 2007.

[6] W. Liu et al., “Heart rate variability at different thermal comfort levels”, *Eur J Appl Physiol*, vol. 103, pp. 361–366, 2008.

[7] M. Malik, A.J. Camm, J. T. Bigger, G. Breithardt et al., “Heart rate variability. Standards of measurement, physiological interpretation, and clinical use”, *European Heart Journal*, vol 17, pp. 354-381, 1996.

[8] A. Khandoker, C. Karmakar, A. Voss, M. Palaniswami, “Poincaré Plot Methods for Heart Rate Variability Analysis”, 2013.

[9] C. Ekici, “A review of thermal comfort and method of using Fanger's PMV equation”, *5th International Symposium on Measurement, Analysis and Modelling of Human Functions,* pp. 61-64, 2013.

[10] M. Humphreys, F. Nicol, “The validity of ISO-PMV for predicting comfort votes in every-day thermal environments”, *Energy and Buildings*, vol. 34, pp. 667-684, 2002.

[11] J. Kim, Y. Zhou, S. Schiavon, P. Raftery, G. Brager, “Personal comfort models: Predicting individuals' thermal preference using occupant heating and cooling behavior and machine learning”, *Building and Environment 129*, pp. 96-106, 2017.

[12] W. Yu et al., “Research on Indoor Thermal Environment Control and Thermal Sensation Prediction”, *IOP Conference Series: Earth and Environmental Science*, 2019.

[13] S. Liu et al., “Personal thermal comfort models based on physiological parameters measured by wearable sensors”, *10th Windsor Conference*, 2018.

[14] C. Z. Dai, H. Zhang, E. Arens, Z. Lian, “Machine learning approaches to predict thermal demands using skin temperatures: Steady-state conditions”, *Building and Environment*, pp. 114: 1─10, 2017.

[15] R. Maiti, “Physiological and subjective thermal response from Indians”, *Build. Environ,* vol. 70, pp. 306-317, 2013.

[16] N. Gerrett, “Body mapping of perceptual responses to sweat and warm stimuli and their relation to physiological parameters”, Thesis, 2012.

[17] N. Gerrett, B. Redortier, T. Voelcker, G. Havenith, “A comparison of galvanic skin conductance and skin wettedness as indicators of thermal discomfort during moderate and high metabolic rates”, *Journal of Thermal Biology*, vol. 38, pp. 530-538, 2013.

[18] F. Pietroni, S. Casaccia, L. Scalise, G. Revel, “Identification of Users’ Well-Being Related to External Stimuli: A Preliminary Investigation”, *CNS 2018: Sensors*, pp 579-590, 2019.

[19] R. Phitayakorn, R. D. Minehart, M. C. M. Pian-Smith, M. W. Hemingway, E. R. Petrusa, “Practicality of using galvanic skin response to measure intraoperative physiologic autonomic activation in operating room team members,” *Surg.*, vol. 158, no. 5, pp. 1415-1420, 2015.

[20] D. R. Bach et al., “Stress detection from speech and galvanic skin response signals,” *J. Neurosci. Methods*, vol. 3820, no. November, pp. 209-214, 2013.

[21] M. Liu, D. Fan, X. Zhang, X. Gong, “Human Emotion Recognition Based on Galvanic Skin Response Signal Feature Selection and SVM,” *2016 International Conference on Smart City and Systems Engineering (ICSCSE)*, pp. 157-160, 2016.

[22] J. Xiong, Z. Lian, X. Zhou, J. You, Y. Lin, “Effects of temperature steps on human health and thermal comfort”, *Build. Environ.,* vol. 94, pp. 144-154, 2015.

[23] J. Xiong, Z. Lian, H. Zhang, “Physiological response to typical temperature step-changes in winter of china”, *Energy Build*., vol. 138, pp. 687-694, 2017.

[24] J. Xiong, Z. Lian, X. Zhou, J. You, Y. Lin, “Potential indicators for the effect of temperature steps on human health and thermal comfort”, *Energy Build*., vol. 113, pp. 87-98, 2016.

[25] K. N. Nkurikiyeyezu et al., “Heart rate variability as a predictive biomarker of thermal comfort”, *J Ambient Intell Human Comput*, vol. 9, pp. 1465–1477, 2018.

[26] K. N. Nkurikiyeyezu et al., “Toward a Real-Time and Physiologically Controlled Thermal Comfort Provision in Office Build”, *Intelligent Environments 2018*, pp. 168-177, 2018.

[27] T. Yao et al., “Experimental study on physiological responses and thermal comfort under various ambient temperatures”, *Physiology & behaviour*, vol. 93, pp. 310-321, 2008.

[28] H. Zhu et al., “Experimental study on the human thermal comfort based on the heart rate variability (HRV) analysis under different environments”, *Science of The Total Environment*, vol. 616–617, pp. 1124-1133, 2018.

[29] T. Deboer, I. Tobler, “Temperature dependence of EEG frequencies during natural hypothermia”, *Brain Res,* vol 670, pp. 153-156, 1995.

[30] T. Deboer, “Electroencephalogram theta frequency changes in parallel with euthermic brain temperature”, *Brain Res*, vol. 930, pp. 212-215, 2002.

[31] Y. Yao, Z. Lian, W. Liu, C. Jiang, Y. Liu, H. Lu, “Heart rate variation and electroencephalograph - the potential physiological factors for thermal comfort study”, *Indoor Air*, vol. 19, pp. 93-101, 2009.

[32] Y. Choi, M. Kim, C. Chun, “Measurement of occupants' stress based on 20 electroencephalograms (EEG) in twelve combined environments”, *Build. Environ. 88*, vol. 21, pp. 65-72, 2015.

[33] X. Shan, E. Yang, J. Zhou, V. Chang, “Human-building interaction under various indoor temperatures through neural-signal electroencephalogram (EEG) methods”, *Building and Environment*, vol. 129, pp. 1-31, 2017.

[34] K. Kanosue, N. Sadato, T. Okada et al., “Brain activation during whole body cooling in humans studied with functional magnetic resonance imaging”, *Neurosci Lett*., vol. 329, pp. 157-160, 2002.

[35] T. Chaudhuri, Y. C. Soh, H. Li, L. Xie, "Machine learning based prediction of thermal comfort in buildings of equatorial Singapore", *2017 IEEE International Conference on Smart Grid and Smart Cities (ICSGSC)*, pp. 72-77, 2017.

[36] T. Tamura, Y. Maeda, M. Sekine, M. Yoshida, “Wearable photoplethysmographic sensors-Past and present”, *Electronics*, vol.3, pp. 282-302, 2014.

[37] N. Selvaraj, A. Jaryal, J. Santhosh, K. K. Deepak, S. Anand, “Assessment of heart rate variability derived from finger-tip photoplethysmography as compared to electrocardiography”, *Journal of Medical Engineering & Technology*, vol. 32, pp. 479-484, 2008.

[38] K. Georgiou, A. Larentzakis, N. Khamis et al., “Can Wearable Devices Accurately Measure Heart Rate Variability? A Systematic Review”, *Folia medica*, vol. 60, pp. 7-19, 2018.

[39] K. F. Tsoi, J.Y.H. Wong, M.P.F. Wong, G.K.S. Leung, B.K.K. Bat, F.C.H. Chan, Y. Kuo, H.H.M. Lo, H.M.L. Meng, “Personal Wearable Devices to Measure Heart Rate Variability: A Framework of Cloud Platform for Public Health Research”, *Proceedings of the 2017 International Conference on Digital Health (DH ’17), Association for Computing Machinery*, pp. 207-208, 2017.

[40] G. Cosoli, S. Spinsante, L. Scalise, “Wrist-worn and chest-strap wearable devices: systematic review on accuracy and metrological characteristics”, *Measurement*, vol 159, pp. 1-15, 2020.

[41] Y. Zhao, P. V. Genovese, Z. Li, “Intelligent Thermal Comfort Controlling System for Buildings Based on IoT and AI”, *Future Internet*, vol. 12, pp. 1-30, 2020.

[42] Y. Yang et al., “Study on Thermal Comfort Model Based on Genetic Algorithm with Backpropagation Neural Network”, *Advancements in Smart City and Intelligent Building*, pp. 23-33, 2019.

[43] D. Megan, P. Raftery, J. Woolley, F. Bauman, “Comparison of mean radiant and air temperatures in mechanically-conditioned commercial buildings from over 200000 field and laboratory measurements”, *Energy and Buildings,* vol. 206, 2019.

[44] V. Földváry, T. Cheung, H. Zhang, R. de Dear, T. Parkinson, E. Arens, C. Chun, S. Schiavon, M. Luo, G. Brager, P. Li, S. Kaam et al., "Development of the ASHRAE Global Thermal Comfort Database II", *Building and Environment*, vol. 142, 2018.

[45] J. Woolley, S. Schiavon, F. Bauman, P. Raftery, J. Pantelic, "Side-by-side laboratory comparison of space heat extraction rates and thermal energy use for radiant and all air systems", *Energy and Buildings*, vol. 176, pp. 139-150, 2018.

[46] D. Robotics UK, "DHT11 Humidity & Temperature Sensor", 2010.

[47] Task Force of the European Society of Cardiology and the North American Society of Pacing and Electrophysiology, "Heart rate variability: standards of measurement, physiological interpretation and clinical use", *Circulation*, vol. 93, pp. 1043–1065, 1996.

[48] T. K. Ho, "Random Decision Forests", *Proceedings of the 3rd International Conference on Document Analysis and Recognition*, pp. 278–282, 1995.

[49] B. Kusy, R. Rana, P. Valencia, R. Jurdak, J. Wall, "Experiences with Sensors for Energy Efficiency in Commercial Buildings", *Lecture Notes in Electrical Engineering*, vol. 281, pp. 231-243, 2014.

[50] R. Rana, B. Kusy, R. Jurdak, J. Wall, W. Hu, "Feasibility analysis of using humidex as an indoor thermal comfort predictor", *Energy and Buildings*, vol. 64, pp. 17–25, 2013.

[51] C. D. Lewis, "Industrial and Business Forecasting Methods", *Butterworths Publishing*, 1982.